

Selectron Pair Production in e^+e^- Colliders and the Supergravity Spectrum

Beatriz de Carlos [†] and **Marco A. Díaz** [‡]

[†] School of Mathematical and Physical Sciences, University of Sussex
 Falmer, Brighton BN1 9QH, U.K.
 e-mail: B.de-Carlos@sussex.ac.uk

[‡] Physics Department, University of Southampton
 Southampton, SO17 1BJ, U.K.
 e-mail: mad@hep.phys.soton.ac.uk

Abstract

Selectrons may be produced in pairs at LEP II if their mass is less than about 100 GeV. Preferably, they decay into the lightest neutralino plus an electron. In a scenario where selectrons are observed at LEP II, we show that:

- (i) in a first stage where experimental errors are large, the measurement of the total cross section of selectron pair production, the selectron mass, and the lightest neutralino mass, allow us to validate or rule out the Minimal Supergravity Model in its simplest form, and that
- (ii) in a second stage where precision measurements are available, the value of $\tan \beta$ can be determined together with the rest of the parameters that specify the Minimal Supergravity Model and, with them, the entire supersymmetric spectrum can be calculated.

We include experimental constraints from sparticle searches, Z -pole physics, stability of the lightest supersymmetric particle (LSP) and the decay $b \rightarrow s\gamma$. In these scenarios, small values of $\tan \beta$ and negative values of μ are preferred, and the lightest Higgs mass satisfies $m_h < 110$ GeV, which makes it likely to be detected at LEP II.

1 Introduction

Despite the success of the Standard Model (SM) in describing the strong and electroweak interactions at energy scales accessible to present colliders, this model is regarded as an incomplete theory. Two of the main theoretical problems with the SM are related to the electroweak symmetry breaking. First, it is hard to understand why the scale of electroweak symmetry breaking is much smaller compared to the Planck scale. Second, the existence of fundamental scalars in the SM model is problematical since their masses are unstable under radiative corrections. Both problems are potentially solved in supersymmetric theories. For this and other reasons, since its discovery [1], supersymmetry has received great attention and has become the leading candidate for physics beyond the SM.

The simplest supersymmetric extension of the SM is called the Minimal Supersymmetric Model (MSSM) [2] and it is based on R-parity conservation and minimal particle content. Many experiments have looked for supersymmetric particles, but no signal has been found so far [3, 4, 5]. The e^+e^- annihilation is a clean environment for searching for new particles, and the LEP II collider will have enough energy to look for supersymmetric particles with mass up to about half the center of mass energy, since they are produced in pairs. Besides the lightest Higgs boson, candidates to be found at LEP II are charginos, neutralinos, and sleptons because they are typically lighter than other susy particles. Among them, the cleanest signatures are produced by charged particles: charginos and charged sleptons.

If a supersymmetric particle is detected at LEP II, it is crucial to know what can be learned about the model from the LEP measurements. In the case of chargino pair production, this issue was addressed recently in the case of global supersymmetry [6, 7]. Furthermore, in supergravity (SUGRA) models with radiatively broken electroweak symmetry, the predictions are more powerful [8]. Nevertheless, charged sleptons can be lighter than charginos, and for this reason a charged slepton may be the first supersymmetric signal to be detected.

In supergravity models with radiatively broken electroweak symmetry, selectrons are in general not lighter than staus and smuons and, therefore, the latter may be detected first. But staus and smuons can be produced in e^+e^- colliders only with intermediate photons and Z -bosons in the s -channel. Furthermore, couplings of charged sleptons to γ or Z depend only on electroweak parameters like the gauge coupling constant g , the weak mixing angle θ_W , or the electric charge e . This implies that other than the mass of the stau or smuon, and the mass of the decay products (lightest neutralino), it will be hard to extract more information on the supersymmetric parameters of the model with the discovery of these particles. This is not the case with selectrons. In addition to intermediate γ and Z -bosons, selectrons may be produced in e^+e^- colliders with intermediate neutralinos in the t -channel, and therefore, its production cross section depends on the neutralino sector and is sensible to important supersymmetric parameters.

In global supersymmetry, many authors have studied the selectron pair production in e^+e^- colliders [9], and also the production of off-shell selectrons [10]. The purpose of this paper is to study this process in the context of supergravity models, where the parameters are tightly constrained, and therefore the predictive power is greater. We will demonstrate that the experimental observables associated with the detection of a

pair of selectrons, *i.e.*, the total production cross section, the mass of the selectron, and the mass of its main decay product, the lightest neutralino, allow us to calculate the supersymmetric parameters that define the model, and through them, to predict the entire supersymmetric spectrum.

2 Minimal Supergravity

Minimal Supergravity is defined by a Kähler potential $K = \sum_j |\phi_j|^2$ and a gauge kinetic function $f_{ab} = \delta_{ab}$ so that all the kinetic terms are canonical. The supersymmetric lagrangian is specified by the superpotential W given by¹

$$W = \varepsilon_{ab} \left[h_U^{ij} \widehat{Q}_i^a \widehat{U}_j \widehat{H}_2^b + h_D^{ij} \widehat{Q}_i^b \widehat{D}_j \widehat{H}_1^a + h_E^{ij} \widehat{L}_i^b \widehat{R}_j \widehat{H}_1^a \right] - \mu \varepsilon_{ab} \widehat{H}_1^a \widehat{H}_2^b \quad (1)$$

where $i, j = 1, 2, 3$ are generation indices, $a, b = 1, 2$ are $SU(2)$ indices, and ε is a completely antisymmetric 2×2 matrix, with $\varepsilon_{12} = -\varepsilon_{21} = 1$ and $\varepsilon_{11} = \varepsilon_{22} = 0$. The symbol “hat” over each letter indicates a superfield, with \widehat{Q}_i , \widehat{L}_i , \widehat{H}_1 , and \widehat{H}_2 being $SU(2)$ doublets with hypercharges $\frac{1}{3}$, -1 , -1 , and 1 respectively, and \widehat{U} , \widehat{D} , and \widehat{R} being $SU(2)$ singlets with hypercharges $-\frac{4}{3}$, $\frac{2}{3}$, and 2 respectively. The couplings h_U , h_D and h_E are 3×3 Yukawa matrices, and μ is a parameter with units of mass.

In the supersymmetric part of the lagrangian, we find the Yukawa interactions \mathcal{L}_Y and the scalar potential V_s . In \mathcal{L}_Y we get fermion mass terms and fermion-fermion-scalar interactions, and is given by

$$\mathcal{L}_Y = -\frac{1}{2} \sum_{n,m} \frac{\partial^2 \widetilde{W}}{\partial A_n \partial A_m} \psi_n \psi_m + \text{h.c.} \quad (2)$$

where the function \widetilde{W} is obtained by taking the superpotential in eq. (1) and replacing each superfield by its scalar component. The indices n and m run over all the superfields in the superpotential, and A_n (ψ_n) are the scalar (fermionic) component of each superfield.

The scalar potential V_s consists of two parts, the F terms and the D terms

$$V_s = \sum_n F_n^* F_n + \frac{1}{2} [D^a D^a + (D')^2] \quad ; \quad (3)$$

the F term is given by

$$F_n = \frac{\partial \widetilde{W}}{\partial A_n} \quad , \quad (4)$$

where n runs over all the superfields in eq. (1), and A_n is the corresponding scalar component. The two D terms, one for $SU(2)$ and one for $U(1)$, are

$$D^a = \frac{1}{2} g \sum_n A_n^{i*} \sigma_{ij}^a A_n^j \quad , \quad D' = \frac{1}{2} g' \sum_m y_m A_m^* A_m \quad . \quad (5)$$

The first one is the $SU(2)$ D-term, where n runs over all the superfields which are doublets under $SU(2)$, A_n is the corresponding scalar component, σ^a are the Pauli matrices, and $i, j = 1, 2$ are $SU(2)$ indices. The second is the $U(1)$ D-term, where m runs

¹ We are using here the notation of ref. [11]. We advise the reader that the sign of the μ term in the original version of this paper was corrected in a subsequent erratum.

over all the superfields with a non-zero hypercharge y_m , and A_m is the corresponding scalar component.

Supersymmetry must be broken because otherwise the known fermions would be degenerate in mass with its superpartners and this is not observed experimentally. The actual supergravity mechanism is unknown², but can be parametrized with a set of soft supersymmetry breaking terms which do not introduce quadratic divergences to the unrenormalized theory [13]

$$\begin{aligned} V_{soft} = & \varepsilon_{ab} \left[A_U^{ij} h_U^{ij} \tilde{Q}_i^a \tilde{U}_j H_2^b + A_D^{ij} h_D^{ij} \tilde{Q}_i^b \tilde{D}_j H_1^a + A_E^{ij} h_E^{ij} \tilde{L}_i^b \tilde{R}_j H_1^a \right] - B\mu \varepsilon_{ab} H_1^a H_2^b \\ & + M_Q^{ij2} \tilde{Q}_i^{a*} \tilde{Q}_j^a + M_U^{ij2} \tilde{U}_i^* \tilde{U}_j + M_D^{ij2} \tilde{D}_i^* \tilde{D}_j + M_L^{ij2} \tilde{L}_i^{a*} \tilde{L}_j^a + M_R^{ij2} \tilde{R}_i^* \tilde{R}_j \\ & + m_1^2 H_1^{a*} H_1^a + m_2^2 H_2^{a*} H_2^a - \left[\frac{1}{2} M_s \lambda_s \lambda_s + \frac{1}{2} M \lambda \lambda + \frac{1}{2} M' \lambda' \lambda' + h.c. \right]. \end{aligned} \quad (6)$$

In Minimal Supergravity the scalar masses, the gaugino masses, and the trilinear couplings are universal at the unification scale M_X

$$\begin{aligned} M_Q^{ij2} = M_U^{ij2} = M_D^{ij2} = M_L^{ij2} = M_R^{ij2} = m_0^2 \delta^{ij}, \quad m_1^2 = m_2^2 = m_0^2, \\ M_s = M = M' = M_{1/2}, \quad A_U^{ij} = A_D^{ij} = A_E^{ij} = A \delta^{ij} \end{aligned} \quad (7)$$

and the mass parameters A and B are related to each other at the scale M_X by

$$A = B + m_0. \quad (8)$$

In this case, only four parameters specify the model: the universal scalar mass m_0 , the universal gaugino mass $M_{1/2}$, the universal trilinear coupling A , and the Higgs mass parameter μ .

2.1 The Effective Potential

The Higgs sector of the MSSM [14] contains two Higgs doublets H_1 and H_2 , with hypercharges -1 and 1 respectively, and with the following tree level Higgs potential:

$$\begin{aligned} V_H = & m_{1H}^2 |H_1|^2 + m_{2H}^2 |H_2|^2 - m_{12}^2 (\varepsilon_{ab} H_1^a H_2^b + h.c.) \\ & + \frac{1}{8} (g^2 + g'^2) \left[|H_1|^2 - |H_2|^2 \right]^2 + \frac{1}{2} g^2 |H_1^{a*} H_2^a|^2, \end{aligned} \quad (9)$$

where $m_{1H}^2 = m_1^2 + \mu^2$, $m_{2H}^2 = m_2^2 + \mu^2$, and $m_{12}^2 = B\mu$. This potential has a minimum that breaks the symmetry and the neutral component of the Higgs fields get a vacuum expectation value:

$$H_1 = \begin{pmatrix} \frac{1}{\sqrt{2}} [\chi_1^0 + v_1 + i\varphi_1^0] \\ H_1^- \end{pmatrix}, \quad H_2 = \begin{pmatrix} H_2^+ \\ \frac{1}{\sqrt{2}} [\chi_2^0 + v_2 + i\varphi_2^0] \end{pmatrix}, \quad (10)$$

where $v_1^2 + v_2^2 = (246 \text{ GeV})^2$ is our normalization.

The one-loop effective potential [15], working in dimensional reduction [16], is given by

$$V_{eff} = V_0(v_1, v_2, Q) + \sum_i \frac{w_i}{64\pi^2} m_i^4(v_1, v_2) \left(\ln \frac{m_i^2(v_1, v_2)}{Q^2} - \frac{3}{2} \right). \quad (11)$$

²For an example, see ref. [12].

The index i runs over all the particles of the model, $m_i(v_1, v_2)$ is the mass of the i -th particle as a function of the two vacuum expectation values, and w_i takes into account the internal degrees of freedom of each particle: $w_i = (-1)^{2s}(2s+1)rc$, where s is the spin of the particle, $r = 1(2)$ if the field is real (complex), and c is the color factor. The tree level effective potential is found from eq. (9) after replacing the Higgs fields by their vacuum expectation values:

$$V_0(v_1, v_2, Q) = \frac{1}{32}(g^2 + g'^2)(v_1^2 - v_2^2)^2 + \frac{1}{2}m_{1H}^2 v_1^2 + \frac{1}{2}m_{2H}^2 v_2^2 - m_{12}^2 v_1 v_2. \quad (12)$$

In \overline{DR} , one-loop contributions to the effective potential are explicitly scale dependent and, therefore, the tree level potential $V_0(v_1, v_2, Q)$ must be implicitly scale dependent, *i.e.*, each parameter in the right hand side of eq. (12) is a running parameter governed by a renormalization group equation (RGE).

The electroweak symmetry is broken radiatively because, despite the fact that $m_1^2(Q = M_X) = m_2^2(Q = M_X) = m_0^2$, the large value of the top quark mass makes the RGE of these two mass parameters to evolve differently and $m_2^2(Q)$ is driven towards zero when the scale approaches the weak scale. It was proven that, due to the strong scale dependence of $V_0(v_1, v_2, Q)$, one-loop contributions to the effective potential are important [17], and to find reliable results in the electroweak symmetry breaking, the one-loop contributions from all the particles should be included [18]. One of the free parameters must be fixed in order to reproduce the correct value for the Z -boson mass. We choose to fix $|\mu|$, therefore the model is specified by m_0 , $M_{1/2}$, $\tan\beta$, and $\text{sign}(\mu)$ (we have eliminated A in favor of $\tan\beta$). In our calculations, we use the full one-loop effective potential including the effect of all the particles in the model. We minimize the potential at the scale \hat{Q} defined by the scale where the tree level vacuum expectation values are equal to the one-loop corrected vev's. At this scale we find the running CP-odd Higgs mass $m_A(\hat{Q})^3$, which is related to the pole mass m_A through the relation

$$m_A^2 = m_A^2(\hat{Q}) - (\delta m_A^2)^{\overline{DR}} + A_{AA}(p^2 = m_A^2, \hat{Q}). \quad (13)$$

The function $A_{AA}(p^2, Q)$ is the CP-odd Higgs self energy evaluated at an external momentum p and at an arbitrary scale Q . This function is divergent and its contribution from loops involving top and bottom quarks and squarks is given in the appendix. In \overline{DR} , the mass counterterm δm_A^2 is chosen in such a way that cancels exactly the divergences from the self energy. In addition, the explicit scale dependence of the self energy is canceled by the implicit scale dependence of the running mass parameter $m_A^2(Q)$. In this way, the pole mass m_A^2 is finite and scale independent (up to two-loop effects).

3 Low Energy Spectrum

The two sleptons \tilde{l}_L^\pm and \tilde{l}_R^\pm are the supersymmetric partners of the left and right handed leptons and, in general, they can mix. The mass eigenstates are denoted \tilde{l}_1^\pm and \tilde{l}_2^\pm and the mass matrix is given by

$$\mathbf{M}_{\tilde{l}^\pm}^2 = \begin{bmatrix} M_L^2 + m_l^2 - \frac{1}{2}(2m_W^2 - m_Z^2)c_{2\beta} & m_l(A_l - \mu t_\beta) \\ m_l(A_l - \mu t_\beta) & M_R^2 + m_l^2 - (m_Z^2 - m_W^2)c_{2\beta} \end{bmatrix}. \quad (14)$$

³The scale \hat{Q} is the only point where the running CP-odd Higgs mass is equal to its tree level value $m_A^2(\hat{Q}) = m_{1H}^2(\hat{Q}) + m_{2H}^2(\hat{Q})$.

In the case of selectrons, mixing can be neglected and the mass eigenstates are \tilde{e}_L^\pm and \tilde{e}_R^\pm . Their masses, together with the sneutrino mass, are

$$\begin{aligned} m_{\tilde{e}_L^\pm}^2 &= M_L^2 - \frac{1}{2}(2m_W^2 - m_Z^2)c_{2\beta}, \\ m_{\tilde{e}_R^\pm}^2 &= M_R^2 - (m_Z^2 - m_W^2)c_{2\beta}, \\ m_{\tilde{\nu}_e}^2 &= M_L^2 + \frac{1}{2}m_Z^2c_{2\beta}. \end{aligned} \quad (15)$$

As explained in the previous section, the two soft supersymmetry breaking terms M_L^2 and M_R^2 are equal to m_0 at the unification scale (here we are omitting the generation indices). The solution of the RGE of these two parameters [19] can be approximated by

$$\begin{aligned} M_L^2(m_Z^2) &\approx m_0^2 + \frac{1}{16\pi^2}(3g^2 + g'^2)M_{1/2}^2 \ln \frac{M_X^2}{m_Z^2} \\ M_R^2(m_Z^2) &\approx m_0^2 + \frac{1}{4\pi^2}g'^2M_{1/2}^2 \ln \frac{M_X^2}{m_Z^2}, \end{aligned} \quad (16)$$

implying that M_L^2 is larger than M_R^2 . In addition, since the radiative breaking of the electroweak symmetry can be properly obtained if $\tan\beta > 1$, we infer from eq. (15) that $m_{\tilde{e}_R^\pm} < m_{\tilde{e}_L^\pm}$, and for this reason, we concentrate on the production of $\tilde{e}_R^+\tilde{e}_R^-$ pairs.

Negative searches of charged sleptons [4, 5, 20, 21] impose an experimental lower bound on their mass given by $m_{\tilde{l}^\pm} > 45$ GeV. Because τ^\pm has a mass much larger than the rest of the leptons, stau mixing is larger and, consequently, τ_1^\pm is in general the lightest of the charged sleptons. In this way, the constraint $m_{\tilde{\tau}^\pm} > 45$ GeV eliminates part of the parameter space. On the other hand, a lower bound on the sneutrino mass is obtained from negative experimental searches [4, 5, 22]. If the three sneutrino flavors are degenerate, the mass has to satisfy $m_{\tilde{\nu}} > 41.8$ GeV, and this is the case in minimal supergravity because the slepton masses are equal to m_0 at the unification scale and the RGE evolve them almost equally. This constraint also reduces the allowed parameter space.

The supersymmetric partners of the W_μ^\pm gauge bosons and the charged Higgs bosons mix to form charginos $\chi_{1,2}^\pm$, whose mass matrix is

$$\mathbf{M_C} = \begin{bmatrix} M & \sqrt{2}m_W s_\beta \\ \sqrt{2}m_W c_\beta & \mu \end{bmatrix}. \quad (17)$$

This matrix is diagonalized by two unitary matrices V and U chosen such that

$$\mathbf{U}^* \mathbf{M_C} \mathbf{V}^{-1} = \mathbf{M_C^d}, \quad (18)$$

where $\mathbf{M_C^d}$ is a diagonal matrix with non-negative entries. The experimental lower bound on the lightest chargino mass is given by [4, 5, 20, 23] $m_{\chi_1^\pm} > 45$ GeV.

In the same way, the supersymmetric partners of the B_μ and W_μ^3 gauge bosons, and the neutral Higgs bosons mix to form the neutralinos χ_j^0 , $j = 1, \dots, 4$. The mass matrix is

$$\mathbf{M_N} = \begin{bmatrix} M' & 0 & -m_Z s_W c_\beta & m_Z s_W s_\beta \\ 0 & M & m_Z c_W c_\beta & -m_Z c_W s_\beta \\ -m_Z s_W c_\beta & m_Z c_W c_\beta & 0 & -\mu \\ m_Z s_W s_\beta & -m_Z c_W s_\beta & -\mu & 0 \end{bmatrix}, \quad (19)$$

and can be diagonalized by a matrix N in this basis, or by a matrix N' in the basis Photino-Zino-Higgsino, according to the notation of ref. [11]. The matrices N and N' can be complex, and they are chosen in such a way that the eigenvalues are real and positive. An equivalent way to diagonalize the neutralino mass matrix is allowing the eigenvalues to be negative: in this case, the matrix N (N') is replaced by the real matrix Z (Z'), and with the neutralino masses we make the replacement $m_{\chi_i^0} \longrightarrow \epsilon_i m_{\chi_i^0}$, where ϵ_i is the sign of the i -th eigenvalue and the neutralino masses are positive.

Negative experimental searches impose a $\tan\beta$ dependent lower bound on the lightest neutralino mass [5, 24]. With the extra assumption of gaugino universality, lower bounds on the heavier neutralinos (and heavy chargino) can be set [25] with the help of gluino searches [26]. Equivalently, we prefer to impose that the 95% CL upper bound on the contribution of new particles to the Z width is $\Delta\Gamma_Z < 23.1$ MeV, that the branching fraction for the decays $Z \rightarrow \tilde{\chi}_i^0 \tilde{\chi}_j^0$ (where i and j are not both 1) satisfies $B(Z \rightarrow \tilde{\chi}_i^0 \tilde{\chi}_j^0) < 10^{-5}$, and that the invisible width of the Z satisfies $\Delta\Gamma_Z^{inv} < 8.4$ MeV [27]. A light gluino (with a mass of the order of a few GeV) has not been ruled out by experiments [28], and gaugino universality implies a lightest neutralino with a mass smaller than 1 GeV. Nevertheless, in supergravity models it has been proven that a light gluino is incompatible with the radiatively broken electroweak symmetry [29] (see also [30]), and we do not consider this case here.

The Higgs sector of the MSSM consists of five physical states, two neutral CP-even Higgs bosons h and H , one neutral CP-odd Higgs boson A , and a pair of charged Higgs bosons H^\pm . In an on-shell scheme, where the CP-odd Higgs mass m_A is defined as the pole of the propagator and calculated with eq. (13), and where $\tan\beta$ is defined through the $A\tau^+\tau^-$ vertex [31], we compute all the one-loop renormalized Higgs masses. In the case of the charged Higgs mass m_{H^\pm} , we include [32] exact one-loop contributions from the top-bottom quark-squark sector and leading logarithms from lighter generations of quarks and squarks, three generations of leptons and sleptons, Higgs and gauge bosons, charginos and neutralinos [33, 34]. We find that radiative corrections to the charged Higgs mass are small for the values of $\tan\beta$ we are considering.

In the case of neutral Higgs bosons, radiative corrections are larger since the leading terms are proportional to m_t^4 [34, 35]. Here we include full one-loop contributions from top-bottom quarks and squarks and leading logarithms from the rest of the particles. Two-loop are important [36, 37], and we include the leading contributions valid at any value of $\tan\beta$ [37]. We renormalize the 2×2 inverse propagator matrix of the CP-even neutral Higgs sector using a momentum dependent mixing angle $\alpha(p^2)$ [38], which allows us to calculate the renormalized value of the parameter $\sin(\beta - \alpha)$ at the two physical scales $p^2 = m_h^2$ and $p^2 = m_H^2$. This parameter is important because it is the MSSM coupling of h to two Z -bosons relative to the $H_{SM}ZZ$ coupling, and in the decoupling limit [39] where $\sin(\beta - \alpha) \rightarrow 1$, it will be very difficult to distinguish the MSSM Higgs h from the SM Higgs H_{SM} without other supersymmetric signal⁴.

⁴Nevertheless, the SM with no new physics below $\sim 10^{10}$ GeV and the MSSM with $M_{SUSY} \lesssim 1$ GeV can be distinguished with the measurement of the Higgs mass [40].

4 Selectron Pair Production and Decay

In this section we display the relevant formulas for the total cross sections of selectron pair production in electron-positron annihilation and their subsequent decay. In the following, the index i labels the two different selectrons \tilde{e}_i with $i = L, R$, whose masses are denoted by $m_i^2 \equiv m_{\tilde{e}_i}^2$. Similarly, the index j (as well as k) labels the four different neutralinos χ_j^0 with $j = 1, 4$, whose masses are $m_j^2 \equiv m_{\chi_j^0}^2$. We start with the production of two selectrons of the same type. In this case, there are contributions from intermediate γ and Z bosons in the s-channel, and from neutralinos in the t-channel, as indicated by Figs. 1(a) and 1(b). The two total cross sections can be calculated with the formula:

$$\begin{aligned} \sigma(e^+e^- \longrightarrow \tilde{e}_i^+\tilde{e}_i^-) &= \frac{(1 - 4m_i^2/s)^{3/2}}{24\pi s} \left[\frac{1}{2}e^4 + \frac{g^2 a_i^2}{16c_W^2} (1 - 4s_W^2 + 8s_W^4) \frac{s^2}{P_Z(s)} \right. \\ &+ \left. \frac{e^2 g a_i}{2c_W} \left(\frac{1}{2} - 2s_W^2 \right) \frac{s(s - m_Z^2)}{P_Z(s)} \right] - \frac{1}{4\pi s} \sum_{j=1}^4 \sum_{k=1}^4 |\lambda_{ij}|^2 |\lambda_{ik}|^2 h^{ijk} \\ &+ \frac{1}{8\pi s} \sum_{j=1}^4 |\lambda_{ij}|^2 f^{ij} \left[e^2 + a_i^2 \frac{s(s - m_Z^2)}{P_Z(s)} \right] \end{aligned} \quad (20)$$

where s is the center of mass energy. In the first line of this formula, the term proportional to e^4 corresponds to the photon contribution, and the term proportional to g^2 corresponds to the Z contribution, where we have defined the constants a_i by $a_L = g(\frac{1}{2} - s_W^2)/c_W$ and $a_R = -gs_W^2/c_W$, and the denominator $P_Z(s)$ comes from the Z propagator: $P_Z(s) = (s - m_Z^2)^2 + \Gamma_Z^2 m_Z^2$. In the second line, the term proportional to $e^2 g$ is the $\gamma - Z$ interference, and the term with the double sum corresponds to the neutralino sector ($\chi^0 - \chi^0$ term). Here, λ_{ij} are the coefficients in the $e^+ \chi_j^0 \tilde{e}_i^-$ vertex given by

$$\lambda_{Lj} = \frac{1}{\sqrt{2}} [eN'_{j1} + a_L N'_{j2}], \quad \lambda_{Rj} = -\frac{1}{\sqrt{2}} [eN'^*_{j1} + a_R N'^*_{j2}] \quad (21)$$

and the matrix N' is defined below eq. (19).

In the $\chi^0 - \chi^0$ term we also introduce the function h^{ijk} . The definition of this function depends on whether we are considering the interference between two different neutralinos or the amplitude squared of one of them. The expression for h^{ijk} is:

$$h^{ijk} = \begin{cases} -\frac{1}{2} s \frac{f^{ij} - f^{ik}}{m_j^2 - m_k^2} & \text{if } m_j^2 \neq m_k^2 \\ g^{ij} & \text{if } m_j^2 = m_k^2 \end{cases} \quad (22)$$

where the two functions f^{ij} and g^{ij} are given by

$$f^{ij} = \sqrt{1 - 4m_i^2/s} \left(-1 + 2 \frac{\Delta m_{ij}^2}{s} \right) + 2 \left[\frac{m_j^2}{s} + \frac{(\Delta m_{ij}^2)^2}{s^2} \right] \ln \left[\frac{\Delta m_{ij}^2 - \frac{1}{2} s y_+}{\Delta m_{ij}^2 - \frac{1}{2} s y_-} \right] \quad (23)$$

and

$$g^{ij} = 2\sqrt{1 - 4m_i^2/s} + \left(-1 + 2 \frac{\Delta m_{ij}^2}{s} \right) \ln \left[\frac{\Delta m_{ij}^2 - \frac{1}{2} s y_+}{\Delta m_{ij}^2 - \frac{1}{2} s y_-} \right]. \quad (24)$$

In this case, we have defined $\Delta m_{ij}^2 = m_i^2 - m_j^2$ and $y_{\pm} = 1 \pm \sqrt{1 - 4m_i^2/s}$. Finally, the third line in eq. (20) has the $\gamma - \chi^0$ interference, proportional to e^2 , and the $Z - \chi^0$

interference, proportional to a_i^2 . In these terms, the function f^{ij} is the one defined in eq. (23).

Now we turn to the production of two selectrons of a different type. The total cross sections receive contributions only from neutralinos in the t-channel [Fig. 1(b)], and the formulas are simply:

$$\sigma(e^+e^- \longrightarrow \tilde{e}_L^+ \tilde{e}_R^-) = \sigma(e^+e^- \longrightarrow \tilde{e}_R^+ \tilde{e}_L^-) = \frac{1}{4\pi s} \sum_{j=1}^4 \sum_{k=1}^4 \lambda_{Lj} \lambda_{Rj} \lambda_{Lk}^* \lambda_{Rk}^* H^{jk} \quad (25)$$

where the couplings λ_{ij} are defined in eq. (21), and the function H^{jk} is given by:

$$H^{jk} = \begin{cases} -\frac{m_j m_k}{m_j^2 - m_k^2} \left(\ln \left[\frac{\Delta \bar{m}_j^2 - s \bar{y}_+ / 2}{\Delta \bar{m}_j^2 - s \bar{y}_- / 2} \right] - \ln \left[\frac{\Delta \bar{m}_k^2 - s \bar{y}_+ / 2}{\Delta \bar{m}_k^2 - s \bar{y}_- / 2} \right] \right) & \text{if } m_j^2 \neq m_k^2 \\ \lambda_{ad}^{1/2} \frac{m_j^2 s}{(\Delta \bar{m}_j^2 - s \bar{y}_+ / 2)(\Delta \bar{m}_j^2 - s \bar{y}_- / 2)} & \text{if } m_j^2 = m_k^2 \end{cases} \quad (26)$$

This time we define $\Delta \bar{m}_j^2 = \frac{1}{2}(m_L^2 + m_R^2) - m_j^2$ and $\bar{y}_\pm = 1 \pm \lambda_{ad}^{1/2}$. The function λ is well known, $\lambda(a, b, c) = a^2 + b^2 + c^2 - 2ab - 2ac - 2bc$ and the subscript “ad” is used to remind the reader that we have chosen to use adimensional arguments: $\lambda_{ad} = \lambda(1, m_L^2/s, m_R^2/s)$.

The main decay modes of a selectron are neutralinos $\tilde{e}_i^\pm \rightarrow e^\pm \chi_j^0$, charginos $\tilde{e}_i^\pm \rightarrow \nu_e \chi_k^\pm$, and sneutrinos $\tilde{e}_i^\pm \rightarrow W^\pm \tilde{\nu}_e$, where $i = L, R$, $j = 1, \dots, 4$, and $k = 1, 2$. The corresponding decay rates are:

$$\begin{aligned} \Gamma(\tilde{e}_i^- \longrightarrow e^- \chi_j^0) &= \frac{1}{4\pi} |\lambda_{ij}|^2 m_i \left(1 - \frac{m_j^2}{m_i^2} \right)^2 \\ \Gamma(\tilde{e}_L^- \longrightarrow \nu_e \chi_k^-) &= \frac{g^2}{16\pi} |U_{k1}|^2 m_L \left(1 - \frac{m_k^2}{m_L^2} \right)^2 \\ \Gamma(\tilde{e}_L^- \longrightarrow W^- \tilde{\nu}_e) &= \frac{g^2}{32\pi} \frac{m_L^3}{m_W^2} \lambda^{3/2}(1, m_{\tilde{\nu}_e}^2/m_L^2, m_W^2/m_L^2) \end{aligned} \quad (27)$$

where λ_{ij} is defined in eq. (21), the matrix U is defined in eq. (18), and the function $\lambda(a, b, c)$ is defined below eq. (26).

5 Results

Once we have introduced the theoretical framework in which we want to work, we can proceed to present some results; as was mentioned at the end of section 2, our free high-energy parameters, once we take into account the constraints imposed by a correct electroweak breaking, are m_0 , $M_{1/2}$, $\tan \beta$ and $\text{sign}(\mu)$. Let's restrict ourselves, for the moment, to the $\mu < 0$ case: this leaves us with only three parameters, $M_{1/2}$, m_0 and $\tan \beta$. For the purposes of our calculation (that is, to find regions with a non-negligible selectron pair production cross-section) we must choose those values of $M_{1/2}$, m_0 which give rise to the lowest possible values for the selectron masses. Let's stress here that, in a SUGRA model, all the spectrum is correlated, so that every choice of $M_{1/2}$, m_0 and $\tan \beta$ determine the values the masses of *all* the susy particles; so we have to keep in mind their experimental constraints [3] simultaneously.

The regions we have explored can be labeled by their $\tan\beta$ value; once this is specified we have found more intuitive to classify the spectrum by their value for the common gaugino mass, $M_{1/2}$. This is due to the fact that, given a value of $\tan\beta$, the neutralino and chargino mass matrices are determined by the values of $M_{1/2}$ and μ . In these minimal SUGRA models we know that the value of μ is given by the requirement of a correct electroweak breaking (i.e. a correct M_Z), and in fact we have observed that, despite the value of m_0 that we are considering, we need μ to be always larger than $M_{1/2}$. What this is telling us is that the lightest neutralino and chargino are going to be mainly gaugino, so that the lowest experimental bounds on these particles (mainly on neutralinos through the experimental restrictions imposed to the decay of the Z in visible neutralinos, see sect. 3) set a lower bound on the value of $M_{1/2}$ that we are able to take. And this will be between 70 and 100 GeV. In conclusion, given a choice for $\tan\beta$, all the points in our parameter space with a common value for the gaugino mass share the same value for the lightest neutralino and chargino ones, and also for that of the gluino (note that the latter is even almost independent of the value of $\tan\beta$, as can be seen in Table 1). In our case, and for reasons that will become clear soon, we have explored a region of values for $M_{1/2}$ up to 150 GeV.

$M_{1/2}$	$\tan\beta$	$m_{\chi_1^0}$	$m_{\chi_1^\pm}$	$m_{\tilde{g}}$
70	2	32	77	224
80	2	37	83	255
90	2	41	90	286
100	2	45	97	317
150	2	65	135	480
90	10	35	59	286
100	10	40	69	318
120	10	48	87	381
150	10	61	114	478
100	25	37	62	318
120	25	46	81	382

Table 1. Lightest neutralino, lightest chargino and gluino masses (in GeV) for different choices of $M_{1/2}$ and $\tan\beta$, and $\mu < 0$. These masses are independent of the value of m_0 , and because of this, any of them can be used to label the curves we show in Figs. 2–8.

But we still cannot say much about scalar masses, in particular about selectron masses, as we have not specified any value at all for m_0 . This will be given, in its lowest bound, by the experimental bounds on the slepton masses, the lightest among the scalars. For low values of $\tan\beta$ we have a very small mixing in the stau mass matrix, therefore the lightest scalar is the sneutrino (being all selectrons, smuons and staus almost degenerate in mass). Let's note that, as $M_{1/2}$ increases, this lower bound on m_0 decreases, due to the presence of gaugino masses in the RGEs of scalar masses [19] as indicated by eq. (16); in fact for $\tan\beta = 2$ and $M_{1/2} \gtrsim 100$ GeV we find that it practically disappears (i.e. any choice for m_0 gives a spectrum compatible with the experimental bounds).

The behaviour of the different low-energy masses is presented in Figs. 2–6, where the curves are labeled by the corresponding lightest neutralino mass (or, equivalently, by the value of $M_{1/2}$, as can be seen in Table 1). In Figs. 2 and 3 we have plotted

the sneutrino (the three sneutrino species are practically degenerate) and lightest stau masses respectively, and we can clearly appreciate how the experimental lower bounds on their masses restrict the allowed parameter space. In cases (a) $\tan\beta = 2$ and (b) $\tan\beta = 10$, restrictions coming from the sneutrino mass dominate as we see in Fig. 2, where some of the curves are truncated by the condition $m_{\tilde{\nu}} > 41.8$ GeV. We can also see that the range of right-handed selectron mass (plotted in the x-axis), which corresponds to a particular choice of $m_{\chi_1^0}$, increases with this mass until it reaches a maximum. The reason for this is the decrease of the lower bound on m_0 mentioned before: since $m_{\tilde{\nu}}$ receives contributions from $M_{1/2}$ as well as from m_0 , higher values of $M_{1/2}$ allow lower values of m_0 . From eqs. (15) and (16) we get:

$$m_{\tilde{e}_R^\pm}^2 \approx m_{\tilde{\nu}}^2 - \frac{3}{16\pi^2}(g^2 - g'^2)M_{1/2}^2 \ln \frac{M_X^2}{m_Z^2} - \frac{1}{2}(3m_Z^2 - 2m_W^2)c_{2\beta}, \quad (28)$$

and from this equation we see that for a constant value of $\tan\beta$, and for $m_{\tilde{\nu}} = 41.8$ GeV, the minimum selectron mass decreases with an increasing $m_{\chi_1^0}$. After its maximum, the range of $m_{\tilde{e}_R^\pm}$ becomes narrower because the value of $M_{1/2}$ is big enough to be unable to produce light selectrons anymore. This is the reason to limit the plots to $M_{1/2} \leq 150$ GeV.

As the value of $\tan\beta$ increases, the stau mixing also does, and experimental restrictions coming from the stau mass start to dominate; in fact, it can be the case that the stau is lighter than the lightest neutralino, χ_1^0 , becoming thus the lightest supersymmetric particle (LSP). This situation is cosmologically disfavoured [41], so it provides us with a new constraint on our parameter space, which is best appreciated in Fig. 3. For large $\tan\beta$ the lightest stau becomes also the lightest scalar, and we can see from Fig. 3(c) that one of the curves is truncated by the condition $m_{\tilde{\tau}_1^\pm} > 45$ GeV. However, as $M_{1/2}$ increases the mass of the lightest neutralino also does, and for $m_{\chi_1^0} > 45$ GeV, the condition that the LSP has to be electrically neutral imposes $m_{\tilde{\tau}_1^\pm} > m_{\chi_1^0}$. In fact, this latter requirement rules out any spectra with $M_{1/2} = 150$ GeV and $\tan\beta = 25$. Also, in this large $\tan\beta$ regime it is no longer possible to reach values for m_0 as low as in the former cases (where we had small or zero stau mixing). For example, for $\tan\beta = 25$ and $M_{1/2} \geq 100$ GeV, m_0 must be always bigger than 55 GeV⁵. The absence of low values for m_0 sets a minimum in the range of selectron masses that increases uniformly with increasing $m_{\chi_1^0}$.

In Fig. 4 we plot the lightest top and bottom squark masses. Squarks are heavier than sleptons mainly because the RGE of soft squark masses receive contributions from the strong coupling constant. In general bottom squarks are heavier than top squarks, and the reasons are that: i) the sbottom soft mass is larger than the stop one because Yukawa couplings contribute negatively to their RGEs, and ii) the off-diagonal elements of the stop mass matrix (which are proportional to the corresponding Yukawa coupling and $\tan\beta$) are much bigger. The exception occurs in case (a) with light neutralino, where $m_{\tilde{t}_1}$ is smaller than $m_{\tilde{b}_1}$, the reason being that the soft squark masses are comparable to m_t , so that the diagonal elements of the stops are much

⁵ This can be easily seen if we rewrite the condition $m_{\tilde{\tau}_1^\pm}^2 > m_{\chi_1^0}^2$ in terms of the corresponding RGEs for large $\tan\beta$, and taking into account that, in our model, the lightest neutralino is mainly gaugino. Then the relationship between the different parameters is given by: $m_0^2 + 0.23M_{1/2}^2 > 1.75[\mu(m_Z)]\tan\beta$.

bigger than those of the sbottoms. In addition, the small value of $\tan\beta$ makes the off-diagonal term less important (see the squark mass matrices in the appendix).

The Higgs spectrum is presented in Figs. 5 and 6. The masses of the heavy Higgs bosons, given by the CP-odd Higgs A , the charged Higgs H^\pm , and the heavy CP-even Higgs H , are plotted in Fig. 5. In the region of parameter space we are considering here, radiative corrections to m_{H^\pm} and m_H are small, typically not larger than a few GeV. Consequently, the charged Higgs and heavy CP-even Higgs pole masses are, to a good approximation, determined by the values of the pole mass m_A and $\tan\beta$. Similarly, the difference between the pole mass m_A and the running mass $m_A(\hat{Q})$ is small. On the other hand, the running CP-odd Higgs mass $m_A(\hat{Q})$ is determined by the correct radiatively broken electroweak symmetry ($\tan\beta$ is an input). We find that for $\tan\beta = 2$, the CP-odd Higgs is heavier in comparison with higher values of $\tan\beta$, and that increasing values of $M_{1/2}$ produce higher values of m_A .

The lightest Higgs h is massless at tree level if $\tan\beta = 1$, and its mass increases until it saturates as $\tan\beta \rightarrow \infty$. This effect can be appreciated as we compare the three cases $\tan\beta = 2, 10$, and 25 in Fig. 6. Two different effects influence the dependence of the Higgs mass m_h on the lightest neutralino mass. First, if $m_{\chi_1^0}$ increases m_A also does, producing higher values of m_h . Second, larger values of squark masses are obtained if $m_{\chi_1^0}$ increases, producing larger contributions to m_h from radiative corrections. This latest effect can be seen in Fig. 6(c), because at large $\tan\beta$, the lightest Higgs mass m_h becomes independent of m_A at tree level, and equal to m_Z . The difference is due to radiative corrections. From this figure it is obvious the importance of the inclusion of radiative corrections in the calculation of m_h .

A SM Higgs boson can be detected at LEP II if its mass is smaller than about 105 GeV [42] (bremsstrahlung of a Higgs by a Z gauge boson). Since the lightest Higgs mass m_h in Fig. 6 is always lighter than about 110 GeV, if this scenario is correct, it is likely to be observed at LEP II. Production cross sections and decay rates of this supersymmetric Higgs h are close to the ones of the SM Higgs, since the parameter $\sin(\beta - \alpha)$ is always close to one, making difficult to distinguish between the two models [39, 40]. Nevertheless, for values of $m_{\chi_1^0} \lesssim 40$ GeV and $\tan\beta = 10$ or 25 , this parameter can be as small as $\sin(\beta - \alpha) \gtrsim 0.95$, which means that the ratio between the production cross sections of the two models can be as low as $\sigma_{MSSM}/\sigma_{SM} \gtrsim 0.9$ and discrimination may be possible. Production of heavy CP-even Higgs bosons at LEP II will be difficult. In the cases described above, m_H is about 120–130 GeV and $|\cos(\beta - \alpha)| \lesssim 0.3$, which means that its production cross section is about 10% of the SM one.

Once we have calculated both the spectrum and the total cross section, we can present our predictions. Those are shown in Figs. 7(a)–7(c) where we have plotted the total cross section $\sigma(e^+e^- \rightarrow \tilde{e}_R^+ \tilde{e}_R^-)$ (the only relevant one) versus the right-handed selectron mass for a center-of-mass energy of 200 GeV and several choices of the lightest neutralino mass (see caption for details). As was mentioned before, low values for $\tan\beta$ produce smaller values for $m_{\tilde{e}_R^\pm}$, and therefore a higher total cross section. In general we see that, for every $\tan\beta$ value we have examined, the different curves (labeled by their corresponding $m_{\chi_1^0}$ value) tend to be very close to each other making potentially very difficult to identify a particular minimal SUGRA spectrum as the one corresponding to a certain value of both $m_{\tilde{e}_R^\pm}$ and $\sigma(e^+e^- \rightarrow \tilde{e}_R^+ \tilde{e}_R^-)$. But luckily enough we are provided with another tool to tell them apart.

As has been stressed in recent years, the $b \rightarrow s, \gamma$ decay is becoming a very pow-

erful test of physics beyond the Standard Model [19, 43, 44], in particular since the measurement of its branching ratio (BR) by the CLEO collaboration. As a FCNC process, $b \rightarrow s, \gamma$ is forbidden at tree level, so 1-loop diagrams become the dominant ones. In our case the presence of susy particles provides us with an extra contribution to this BR to be added to the usual SM one (given mainly by a top quark and a W^- boson running in the loop); therefore the actual experimental bounds $1 \times 10^{-4} \leq \text{BR}(b \rightarrow s, \gamma) \leq 4.2 \times 10^{-4}$ [45] put strong constraints on the supersymmetric spectrum (for a detailed analysis see refs. [19, 43, 44]), and we have used this fact to discard some of the spectra we have shown in the previous plots. As we can see in Fig. 8, where the predicted BR is plotted for each spectrum we have considered versus the corresponding selectron mass, the bigger $\tan\beta$ is, the less compatible with the experiment the spectra are. While in Fig. 8(a) we see that the lightest neutralino mass curve is very close to the SM prediction, as $\tan\beta$ increases the corresponding line in Fig. 8(b) comes closer to the lower CLEO bound and finally, in 8(c), goes even below it, becoming totally discarded (that being the reason why it has been represented by a dashed-dotted line in Fig. 7).

Pretty much the same happens with the highest neutralino mass line: for increasing $\tan\beta$ it becomes closer and even above the upper CLEO bound. Nevertheless, we are being conservative in our predictions and, considering the estimated 25 % error in the theoretical calculation for the $\text{BR}(b \rightarrow s, \gamma)$, we have kept the highest neutralino mass line for $\tan\beta = 10$ as compatible with the bound⁶ (and therefore represented as a solid line in Figs. 7(b) and 8(b)). In any case it is noticeable how an improvement of the experimental measurement by an order of magnitude would discard most of the parameter space shown in our plots. Note also how the closest prediction to that of the SM corresponds to a heavier spectrum as $\tan\beta$ increases: for $\tan\beta = 2$ we have $m_{\chi_1^0} = 32$ GeV, while for $\tan\beta = 10$ we get $m_{\chi_1^0} = 40$ GeV and for $\tan\beta = 25$, $m_{\chi_1^0} = 46$ GeV. That, combined with the results shown in Fig. 7, tells us that if minimal SUGRA is the theory beyond the SM, a low $\tan\beta$ value is more likely to be discovered at LEP II, since it predicts a much lighter spectrum and a sizable cross section for selectron production than higher values of $\tan\beta$; alternatively the reverse statement does not have to be true, that is the absence of measurements at LEP II would not imply a particular range of values of $\tan\beta$ as the preferred one.

Once selectrons are produced we can examine the decay channels in this Minimal SUGRA model. As we explained in the last section, there are three main possible ways for this to happen. However, taking into account that we are focussing in right handed selectrons (the lightest and, therefore the first ones to be produced), two of the couplings ($\tilde{e}_R^- W^+ \tilde{\nu}_e$ and $\tilde{e}_R^- \nu_e \chi_k^+$) are zero and we are left with neutralinos as the only decaying products. In the scenario we consider here, χ_3^0 and χ_4^0 are too heavy, and these decays are kinematically forbidden. In Fig. 9 we plot the branching ratios of the remaining two decay modes, namely $\tilde{e}_R^\pm \rightarrow e^\pm \chi_j^0$, with $j = 1, 2$. We do not consider cascade decays [46]. The branching ratios are plotted as a function of the selectron mass, in the case $\mu < 0$, and for different values of $\tan\beta$ and $M_{1/2}$. Note that the decay rate of a right selectron to the lightest neutralino becomes dominant at low values of $\tan\beta$ (case 1), where the difference between $m_{\chi_1^0}$ and $m_{\chi_2^0}$ is more pronounced (this

⁶Remember that the equivalent case for $\tan\beta = 25$ was discarded for giving a charged (lightest stau) LSP.

can be checked by looking at Table 1, and taking into account that $m_{\chi_2^0}$ is practically identical to $m_{\chi_1^\pm}$). On the other hand, the decay into the second lightest neutralino is important at high values of $\tan\beta$ and low universal gaugino mass $M_{1/2}$ (cases 2 and 4) for which the magnitudes of the two neutralino masses are closer.

Let's turn now to $\mu > 0$. In this case we have observed a much bigger suppression of the allowed parameter space, as becomes clear from Table 2:

$M_{1/2}$	$\tan\beta$	$m_{\chi_1^0}$	$m_{\chi_1^\pm}$	$m_{\tilde{g}}$
120	2	34	64	382
150	2	51	94	481
100	10	30	52	318
120	10	41	71	381
150	10	56	100	479
100	25	33	56	318
120	25	43	74	382

Table 2. Lightest neutralino, lightest chargino and gluino masses (in GeV) for different choices of $M_{1/2}$ and $\tan\beta$, and $\mu > 0$.

Compared to the $\mu < 0$ case, to produce a spectrum (in particular charginos and neutralinos) which is compatible with all the experimental bounds on susy masses and precision measurements on the Z peak, much bigger values of $M_{1/2}$ are required. In addition, the minimum value of $M_{1/2}$ that fulfills these requirements decreases with increasing $\tan\beta$ as opposed to what happened with $\mu < 0$. Concerning the range of variation of m_0 , it is similar to what we found before: no bound for $\tan\beta = 2$, while for $\tan\beta = 10$ a too light sneutrino imposes $m_0 \geq 30$ GeV for $M_{1/2} = 100$ GeV (and no restrictions for $M_{1/2} = 120, 150$ GeV), and for $\tan\beta = 25$ a too light stau implies $m_0 \geq 55$ GeV for any value of $M_{1/2}$. Furthermore, any spectra with $\tan\beta = 25$ and $M_{1/2} = 150$ GeV is ruled out considering that the LSP is electrically neutral, as it happened with $\mu < 0$. In general we have found that, for a fixed $M_{1/2}$, the spectrum is insensitive to $\text{sign}(\mu)$ when $\tan\beta$ is large, while it becomes lighter for $\mu > 0$ as $\tan\beta$ decreases.

Because values of $M_{1/2}$ as small as in the previous case are not allowed, the CP-odd Higgs mass necessary to obtain a correct electroweak symmetry breaking is larger when $\mu > 0$ and, consequently, the charged Higgs H^\pm and the CP-even Higgs H are heavier. At the same time, the light CP-even Higgs h is heavier because m_A is larger (increasing the tree level mass) and because squarks are heavier (increasing the radiative corrections). In addition, when $\mu > 0$ the Higgs h behaves more like the SM Higgs because a larger m_A produces a value of $\sin(\beta - \alpha)$ closer to unity. Nevertheless, still there are good chances to detect this Higgs boson since its mass remains below 110 GeV.

The total cross section versus the right selectron mass for this case and $\tan\beta = 2, 10, 25$ is presented in Fig. 10(a). As we can see, the most relevant cross sections are already ruled out by considering the restrictions coming from the $b \rightarrow s, \gamma$ decay, Fig. 10(b). As was shown in ref. [44]⁷, for $\mu > 0$ there are no low-energy windows,

⁷We advise the reader that this reference uses the opposite convention on the sign of μ , compared with the one we use here.

that is, regions of the parameter space which give a very light spectrum and still are compatible with the experimental measurement for the $\text{BR}(b \rightarrow s, \gamma)$. Therefore the behaviour of the curves is much more uniform than in the previous case and the bigger $M_{1/2}$ is, the closer its associated BR is to the SM prediction. In this particular case we see that $M_{1/2} = 120$ GeV for $\tan \beta = 2, 10$, and $M_{1/2} = 140$ GeV for $\tan \beta = 25$ are the lowest possible values for which their BR start to be compatible with the experimental bound. However an improvement of this measurement would soon discard most of these scenarios with $\mu > 0$, having perhaps those with $\tan \beta = 2$ as the only surviving ones. In any case let's stress the fact that, in the region of the parameter space so far analyzed, $\mu < 0$ gives a much lighter spectrum and therefore a bigger cross section for the production of selectrons.

If right selectrons are discovered at LEP II, measurements of the total cross section $\sigma(e^+e^- \rightarrow \tilde{e}_R^+ \tilde{e}_R^-)$, the selectron mass $m_{\tilde{e}_R^\pm}$, and the mass of the lightest neutralino $m_{\chi_1^0}$ will be available with some degree of experimental error. By looking at Fig. 11 we can see how these measurements can be used to test the model. In this figure we plot the total cross section as a function of the neutralino mass for constant values of the selectron mass $m_{\tilde{e}_R^\pm} = 78$ and 86 GeV, and both signs of μ . In each case, curves of constant $\tan \beta$ are shown. We appreciate that the dependence of the cross section both on $\tan \beta$ and $\text{sign}(\mu)$ is weak, therefore, in a first stage where experimental errors may be high, we will not be able to predict the value of these important parameters from these measurements alone⁸. Nevertheless, it will be possible to test the model, because the curves corresponding to one value of $m_{\tilde{e}_R^\pm}$ are close together and reasonably apart from the group of curves corresponding to the other value of $m_{\tilde{e}_R^\pm}$. For this to happen, there is a maximum tolerable experimental error on the selectron mass which is obvious from the figure. In the next experimental stage, where precision measurements are available, it will be possible to predict both the values of $\tan \beta$ and $\text{sign}(\mu)$.

6 Conclusions

Despite of the multi-dimensional free parameter space that Minimal Supergravity predicts, many phenomenological restrictions can be used altogether to reduce the possible values of the soft terms that define the spectrum. Apart from the direct experimental limits on susy particles and Z-pole physics, we have also imposed constraints coming from a prediction of these spectra for the BR of $b \rightarrow s, \gamma$ compatible with the experimental value, and from the requirement that the LPS should be neutral.

The discovery of selectrons at LEP II will allow us to test the remaining Minimal SUGRA scenarios. In a stage where experimental errors are large, LEP measurements, like the total production cross section $\sigma(e^+e^- \rightarrow \tilde{e}_R^+ \tilde{e}_R^-)$, the selectron mass $m_{\tilde{e}_R^\pm}$, and the lightest neutralino mass $m_{\chi_1^0}$, will validate or rule out the model in its simplest form. In this scenario, other supersymmetric particles are light enough to be produced at LEP II. Among them is the lightest CP-even neutral Higgs boson h , whose discovery and measurement of its mass can give us an important insight into the value of $\tan \beta$ and $\text{sign}(\mu)$. On the other hand, in a stage where precision measurements of the observables mentioned above are available, information on the value of $\tan \beta$ and the

⁸ The observation of the lightest Higgs, for example, can give us information on $\tan \beta$, since m_h depends strongly on this parameter, as we can see from Fig. 6.

sign of μ can be directly obtained, and with it, the entire supergravity spectrum can be predicted.

Acknowledgements

The work of BdeC was supported by a Spanish MEC Postdoctoral Fellowship for most of the time while this research was carried out, and by a PPARC Postdoctoral Fellowship during the final stages of it.

Appendix

The exact one-loop contribution to the CP-odd Higgs self energy from loops involving top and bottom quarks and squarks is given in this appendix using the following independent Veltman's functions [47]:

$$A_0(m^2) = m^2[\Delta - \ln(m^2/Q^2) + 1] \quad (29)$$

$$B_0(p^2; m_1^2, m_2^2) = \Delta - \int_0^1 dx \ln\{[m_2^2 x + m_1^2(1-x) - p^2 x(1-x) - i\varepsilon]/Q^2\}$$

where Q is an arbitrary mass scale, Δ is the regulator of dimensional regularization given by

$$\Delta = \frac{2}{4-n} + \ln 4\pi - \gamma_E, \quad (30)$$

n is the number of space-time dimensions, and γ_E is the Euler's constant.

We denote the sum of the Feynman diagrams contributing to the CP-odd Higgs self energy by $-iA_{AA}(p^2)$. In order to save space we will use the following notation for the Veltman's functions: $A_0(m_a^2) \equiv A_0^a$ and $B_0(p^2; m_a^2, m_b^2) \equiv B_0^{pab}$ where a and b are any particle we are considering.

We begin with the contribution to the CP-odd Higgs self energy from loops involving top and bottom quarks:

$$[A_{AA}(p^2)]^{tb} = \frac{N_c g^2 m_t^2}{32\pi^2 m_W^2 t_\beta^2} (2A_0^t - p^2 B_0^{ptt}) + \frac{N_c g^2 m_b^2 t_\beta^2}{32\pi^2 m_W^2} (2A_0^b - p^2 B_0^{pbb}) \quad (31)$$

with $N_c = 3$ being the number of colors. In the same way, the contribution from top and bottom squarks is

$$\begin{aligned} [A_{AA}(p^2)]^{\tilde{t}\tilde{b}} &= -\frac{N_c}{16\pi^2} \sum_{i=1}^2 \sum_{j=1}^2 (M_{A\tilde{t}\tilde{t}}^{ij})^2 B_0^{p\tilde{t}_i\tilde{t}_j} + \frac{N_c}{16\pi^2} \sum_{i=1}^2 (\lambda_{AA\tilde{t}\tilde{t}}^{ii})^2 A_0^{\tilde{t}_i} \\ &\quad -\frac{N_c}{16\pi^2} \sum_{i=1}^2 \sum_{j=1}^2 (M_{A\tilde{b}\tilde{b}}^{ij})^2 B_0^{p\tilde{b}_i\tilde{b}_j} + \frac{N_c}{16\pi^2} \sum_{i=1}^2 (\lambda_{AA\tilde{b}\tilde{b}}^{ii})^2 A_0^{\tilde{b}_i} \end{aligned} \quad (32)$$

The matrices $M_{A\tilde{t}\tilde{t}}$ and $M_{A\tilde{b}\tilde{b}}$ correspond to the numerical factor in the $A\tilde{t}\tilde{t}$ and $A\tilde{b}\tilde{b}$ Feynman rules in the basis where the squark mass matrices are diagonal. They are given by

$$M_{A\tilde{t}\tilde{t}} = \frac{gm_t}{2m_W}(\mu + A_t/t_\beta) \begin{bmatrix} 0 & -1 \\ 1 & 0 \end{bmatrix}, \quad M_{A\tilde{b}\tilde{b}} = \frac{gm_b}{2m_W}(\mu + A_b t_\beta) \begin{bmatrix} 0 & -1 \\ 1 & 0 \end{bmatrix} \quad (33)$$

In the same way, the matrices $\lambda_{AA\tilde{t}\tilde{t}}$ and $\lambda_{AA\tilde{b}\tilde{b}}$ are the numerical factor in the $AA\tilde{t}\tilde{t}$ and the $AA\tilde{b}\tilde{b}$ vertices in the physical basis, and they are given by

$$\lambda_{AA\tilde{t}\tilde{t}} = R_t \lambda'_{AA\tilde{t}\tilde{t}} R_t^{-1}, \quad \lambda_{AA\tilde{b}\tilde{b}} = R_b \lambda'_{AA\tilde{b}\tilde{b}} R_b^{-1} \quad (34)$$

where $\lambda'_{AA\tilde{t}\tilde{t}}$ and $\lambda'_{AA\tilde{b}\tilde{b}}$ are the equivalent matrices but in the \tilde{t}_L - \tilde{t}_R and \tilde{b}_L - \tilde{b}_R basis

$$\begin{aligned} \lambda'_{AA\tilde{t}\tilde{t}} &= \frac{1}{2}g^2 \begin{bmatrix} \frac{1/2 - e_t s_W^2}{c_W^2} c_{2\beta} - \frac{m_t^2}{m_W^2 t_\beta^2} & 0 \\ 0 & \frac{e_t s_W^2}{c_W^2} c_{2\beta} - \frac{m_t^2}{m_W^2 t_\beta^2} \end{bmatrix} \\ \lambda'_{AA\tilde{b}\tilde{b}} &= \frac{1}{2}g^2 \begin{bmatrix} -\frac{1/2 + e_b s_W^2}{c_W^2} c_{2\beta} - \frac{m_b^2 t_\beta^2}{m_W^2} & 0 \\ 0 & \frac{e_b s_W^2}{c_W^2} c_{2\beta} - \frac{m_b^2 t_\beta^2}{m_W^2} \end{bmatrix}, \end{aligned} \quad (35)$$

and we use the notation $e_t = 2/3$, $e_b = -1/3$, $t_\beta = \tan(\beta)$, and $c_{2\beta} = \cos(2\beta)$. R_t and R_b are rotation matrices defined by

$$R_t = \begin{bmatrix} \cos(\alpha_t) & \sin(\alpha_t) \\ -\sin(\alpha_t) & \cos(\alpha_t) \end{bmatrix}, \quad R_b = \begin{bmatrix} \cos(\alpha_b) & \sin(\alpha_b) \\ -\sin(\alpha_b) & \cos(\alpha_b) \end{bmatrix}, \quad (36)$$

which diagonalize the squark mass matrices

$$R_t M_{\tilde{t}}^2 R_t^{-1} = \begin{pmatrix} m_{\tilde{t}_1}^2 & 0 \\ 0 & m_{\tilde{t}_2}^2 \end{pmatrix}, \quad R_b M_{\tilde{b}}^2 R_b^{-1} = \begin{pmatrix} m_{\tilde{b}_1}^2 & 0 \\ 0 & m_{\tilde{b}_2}^2 \end{pmatrix}, \quad (37)$$

given by

$$\begin{aligned} M_{\tilde{t}}^2 &= \begin{bmatrix} M_Q^2 + m_t^2 + \frac{1}{6}(4m_W^2 - m_Z^2)c_{2\beta} & m_t(A_t - \mu/t_\beta) \\ m_t(A_t - \mu/t_\beta) & M_U^2 + m_t^2 + \frac{2}{3}(m_Z^2 - m_W^2)c_{2\beta} \end{bmatrix} \\ M_{\tilde{b}}^2 &= \begin{bmatrix} M_Q^2 + m_b^2 - \frac{1}{6}(2m_W^2 + m_Z^2)c_{2\beta} & m_b(A_b - \mu t_\beta) \\ m_b(A_b - \mu t_\beta) & M_D^2 + m_b^2 - \frac{1}{3}(m_Z^2 - m_W^2)c_{2\beta} \end{bmatrix}. \end{aligned} \quad (38)$$

where the squark masses M_Q , M_U , and M_D , the trilinear couplings A_t and A_b , and the supersymmetric Higgs mass parameter μ are all defined in section 2.

References

- [1] Yu.A. Gol'fand and E.P. Likhtman, *JETP Lett.* **13**, 323 (1971); D.V. Volkov and V.P. Akulov, *JETP Lett.* **16**, 438 (1972); J. Wess and B. Zumino, *Nucl. Phys. B* **70**, 39 (1974).

- [2] H.P. Nilles, *Phys. Rep.* **110**, 1 (1984); H.E. Haber and G.L. Kane, *Phys. Rep.* **117**, 75 (1985); R. Barbieri, *Riv. Nuovo Cimento* **11**, 1 (1988).
- [3] Review of Particle Properties, *Phys. Rev. D* **50**, 1173 (1994).
- [4] L3 Collaboration (O. Adriani *et al.*), *Phys. Rep.* **236**, 1 (1993).
- [5] The ALEPH Collaboration (D. Decamp *et al.*), *Phys. Rep.* **216**, 253 (1992).
- [6] J. Feng and M. Strassler, *Phys. Rev. D* **51**, 4661 (1995).
- [7] M.A. Díaz and S.F. King, *Phys. Lett. B* **349**, 105 (1995).
- [8] M.A. Díaz and S.F. King, Preprint No. SHEP-95-30, in preparation.
- [9] M.K. Gaillard, L. Hall, and I. Hinchliffe, *Phys. Lett.* **116B**, 279 (1982); M. Glück and E. Reya, *Phys. Lett.* **130B**, 423 (1983); R.M. Barnett, H.E. Haber, and K.S. Lackner, *Phys. Rev. D* **29**, 1381 (1984); T. Schimert and X. Tata, *Phys. Rev. D* **32**, 721 (1985); D.H. Schiller and D. Wöhner, *Nucl. Phys. B* **255**, 505 (1985); T. Kobayashi and M. Kuroda, *Phys. Lett.* **134B**, 271 (1984); A.R. Allan, N. Brown, and A.D. Martin, *Z. Phys. C* **31**, 479 (1986); A. Bartl, H. Fraas, and W. Majerotto, *Z. Phys. C* **34**, 411 (1987); T. Tsukamoto, K. Fujii, H. Murayama, M. Yamaguchi, and Y. Okada, *Phys. Rev. D* **51**, 3153 (1995).
- [10] M. Kuroda, K. Ishikawa, T. Kobayashi and S. Yamada, *Phys. Lett.* **127B**, 467 (1983), Erratum-ibid. **154B**, 457 (1985); I. Hayashibara, F. Takasaki, Y. Shimizu and M. Kuroda, *Phys. Lett.* **158B**, 349 (1985); K. Hidaka, H. Komatsu and P. Ratcliffe, *Nucl. Phys. B* **304**, 417 (1988).
- [11] J.F. Gunion and H.E. Haber, *Nucl. Phys. B* **272**, 1 (1986); erratum-ibid. *B* **402**, 567 (1993).
- [12] B. de Carlos, J.A. Casas and C. Muñoz, *Nucl. Phys. B* **399**, 623 (1993); *Phys. Lett. B* **299**, 234 (1993).
- [13] L. Girardello and M.T. Grisaru, *Nucl. Phys. B* **194**, 65 (1982).
- [14] J.F. Gunion, H.E. Haber, G. Kane and S. Dawson, *The Higgs Hunter's Guide* (Addison-Weslwy, Redwood City, CA, 1990).
- [15] S. Coleman and E. Weinberg, *Phys. Rev. D* **7**, 1888 (1973); S. Weinberg, *Phys. Rev. D* **7**, 2887 (1973).
- [16] W. Siegel, *Phys. Lett.* **84B**, 193 (1979); D.M. Capper, D.R.T. Jones and P. van Nieuwenhuizen, *Nucl. Phys. B* **167**, 479 (1980).
- [17] G. Gamberini, G. Ridolfi and F. Zwirner, *Nucl. Phys. B* **331**, 331 (1990).
- [18] B. de Carlos and J.A. Casas, *Phys. Lett. B* **309**, 320 (1993).
- [19] S. Bertolini, F. Borzumati, A. Masiero, and G. Ridolfi, *Nucl. Phys. B* **353**, 591 (1991).

- [20] DELPHI Collaboration (Abreu *et al.*), *Phys. Lett. B* **247**, 157 (1990); OPAL Collaboration (Akrawy *et al.*), *Phys. Lett. B* **240**, 261 (1990);
- [21] AMY Collaboration (Sakai *et al.*), *Phys. Lett. B* **234**, 534 (1990); VENUS Collaboration (Taketani *et al.*), *Phys. Lett. B* **234**, 202 (1990); TOPAZ Collaboration (Adachi *et al.*), *Phys. Lett. B* **218**, 105 (1989); UA1 Collaboration (Albajar *et al.*), *Z. Phys. C* **44**, 15 (1989).
- [22] DELPHI Collaboration (Abreu *et al.*), *Nucl. Phys. B* **367**, 511 (1991); OPAL Collaboration (Alexander *et al.*), *Z. Phys. C* **52**, 175 (1991).
- [23] TOPAZ Collaboration (Adachi *et al.*), *Phys. Lett. B* **244**, 352 (1990); UA2 Collaboration (Akesson *et al.*), *Phys. Lett. B* **238**, 442 (1990); Mark II Collaboration (Barklow *et al.*), *Phys. Rev. Lett.* **64**, 2984 (1990).
- [24] ASP Collaboration (Hearty *et al.*), *Phys. Rev. D* **39**, 3207 (1989).
- [25] H. Baer, X. Tata, and J. Woodside, *Phys. Rev. D* **44**, 207 (1991); K. Hidaka, *Phys. Rev. D* **44**, 927 (1991).
- [26] CDF Collaboration (Abe *et al.*), *Phys. Rev. Lett.* **69**, 3439 (1992); UA2 Collaboration (Alitti *et al.*), *Phys. Lett. B* **235**, 363 (1990).
- [27] L3 Collaboration (M. Acciarri *et al.*), *Phys. Lett. B* **350**, 109 (1995).
- [28] UA1 Collaboration (C. Albajar *et al.*), *Phys. Lett. B* **198**, 261 (1987); P.M. Tuts *et al.*, *Phys. Lett. B* **186**, 233 (1987).
- [29] M.A. Díaz, *Phys. Rev. Lett.* **73**, 2409 (1994).
- [30] F. de Campos and J.W.F. Valle, Report No. FTUV/93-9, 1993; J.L. Lopez, D.V. Nanopoulos, and X. Wang, *Phys. Lett. B* **313**, 241 (1993); M. Carena, L. Clavelli, D. Matalliotakis, H.P. Nilles, and C.E.M. Wagner, *Phys. Lett. B* **317**, 346 (1993).
- [31] M.A. Díaz, *Phys. Rev. D* **48**, 2152 (1993).
- [32] M.A. Díaz and H.E. Haber, *Phys. Rev. D* **45**, 4246 (1992).
- [33] J.F. Gunion and A. Turski, *Phys. Rev. D* **39**, 2701 (1989); **40**, 2333 (1989); A. Brignole, J. Ellis, G. Ridolfi, and F. Zwirner, *Phys. Lett. B* **271**, 123 (1991); A. Brignole, *Phys. Lett. B* **277**, 313 (1992).
- [34] M.S. Berger, *Phys. Rev. D* **41**, 225 (1990); P.H. Chankowski, S. Pokorski, and J. Rosiek, *Phys. Lett. B* **274**, 191 (1992); K. Sasaki, M. Carena, and C.E.M. Wagner, *Nucl. Phys. B* **381**, 66 (1992); M. Drees and M.M. Nojiri, *Phys. Rev. D* **45**, 2482 (1992); H.E. Haber and R. Hempfling, *Phys. Rev. D* **48**, 4280 (1993).
- [35] H.E. Haber and R. Hempfling, *Phys. Rev. Lett.* **66**, 1815 (1991); A. Yamada, *Phys. Lett. B* **263**, 233 (1991); Y. Okada, M. Yamaguchi and T. Yanagida, *Phys. Lett. B* **262**, 54 (1991); Y. Okada, M. Yamaguchi and T. Yanagida, *Prog. Theor. Phys.* **85**, 1 (1991); J. Ellis, G. Ridolfi and F. Zwirner, *Phys. Lett. B* **257**, 83 (1991); R. Barbieri, M. Frigeni, F. Caravaglios, *Phys. Lett. B* **258**, 167 (1991);

- J. Ellis, G. Ridolfi and F. Zwirner, *Phys. Lett. B* **262**, 477 (1991); J.L. Lopez and D.V. Nanopoulos, *Phys. Lett. B* **266**, 397 (1991); A. Brignole, *Phys. Lett. B* **281**, 284 (1992); D.M. Pierce, A. Papadopoulos, and S. Johnson, *Phys. Rev. Lett.* **68**, 3678 (1992); M.A. Díaz and H.E. Haber, *Phys. Rev. D* **46**, 3086 (1992); A. Yamada, *Z. Phys. C* **61**, 247 (1994); P.H. Chankowski, S. Pokorski, and J. Rosiek, *Nucl. Phys. B* **423**, 437 (1994); A. Dabelstein, *Z. Phys. C* **67**, 495 (1995).
- [36] J.R. Espinosa and M. Quirós, *Phys. Lett. B* **266**, 389 (1991); J. Kodaira, Y. Yasui, and K. Sasaki, *Phys. Rev. D* **50**, 7035 (1994); J.A. Casas, J.R. Espinosa, M. Quirós, and A. Riotto, *Nucl. Phys. B* **436**, 3 (1995); erratum-ibid. *B* **439**, 466 (1995).
- [37] R. Hempfling and A.H. Hoang, *Phys. Lett. B* **331**, 99 (1994).
- [38] M.A. Díaz, preprint VAND-TH-94-19 (hep-ph-9408320), presented at 1994 Meeting of the APS, DPF'94, Albuquerque, New Mexico, 2-6 Aug. 1994.
- [39] H.E. Haber, Santa Cruz Preprint No. SCIPP-94/39, December 1994.
- [40] N.V. Krasnikov and S. Pokorski, *Phys. Lett. B* **288**, 184 (1992); M.A. Díaz, T.A. ter Veldhuis, and T.J. Weiler, *Phys. Rev. Lett.* **74**, 2876 (1995); J.A. Casas, J.R. Espinosa, and M. Quirós, *Phys. Lett. B* **342**, 171 (1995); M.A. Díaz, T.A. ter Veldhuis, and T.J. Weiler, Preprint No. VAND-TH-94-14-REV and SHEP-95-08.
- [41] J. Ellis, J.S. Hagelin, D.V. Nanopoulos, K. Olive and M. Srednicki, *Nucl. Phys. B* **238**, 453 (1984).
- [42] J. F. Gunion, “Searching for the Higgs Boson(s)”, to appear in Proc. of the Zeuthen Workshop — LEP200 and Beyond, Teupitz/Brandenburg, Germany, 10–15 April, 1994, eds. T Riemann and J Blumlein; A. Djouadi, J. Kalinowski and P. M. Zerwas, *Z. Phys.* **C57**, 569 (1993); V. Barger, K. Cheung, A. Djouadi, B. A. Kniehl, and P. M. Zerwas, *Phys. Rev. D* **49**, 79 (1994); A. Djouadi, *Int. J. Mod. Phys.* **A10**, 1 (1995).
- [43] J.L. Hewett, *Phys. Rev. Lett.* **70**, 1045 (1993); V. Barger, M.S. Berger and R.J.N. Phillips, *Phys. Rev. Lett.* **70**, 1368 (1993); M.A. Díaz, *Phys. Lett. B* **304**, 278 (1993); N. Oshimo, *Nucl. Phys.* **B404**, 20 (1993); J.L. Lopez, D.V. Nanopoulos, and G.T. Park, *Phys. Rev. D* **48**, 974 (1993); Y. Okada, *Phys. Lett. B* **315**, 119 (1993); R. Garisto and J.N. Ng, *Phys. Lett. B* **315**, 372 (1993); J.L. Lopez, D.V. Nanopoulos, G.T. Park, and A. Zichichi, *Phys. Rev. D* **49**, 355 (1994); M.A. Díaz, *Phys. Lett. B* **322**, 207 (1994); F.M. Borzumati, *Z. Phys.* **C63**, 291 (1994); S. Bertolini and F. Vissani, *Z. Phys.* **C67**, 513 (1995).
- [44] B. de Carlos and J.A. Casas, *Phys. Lett. B* **349**, 300 (1995); erratum-ibid. *B* **351**, 604 (1995).
- [45] R. Ammar et al. (CLEO Collaboration), *Phys. Rev. Lett.* **71**, 674 (1993); M.S. Alam et al. (CLEO Collaboration), *Phys. Rev. Lett.* **74**, 2885 (1995).
- [46] F. Cuypers, *Phys. At. Nucl.* **56**, 1460 (1993) [*Yad. Fiz.* **56**, 23 (1993)].

[47] G.'t Hooft and M. Veltman, *Nucl. Phys.* **B153**, 365 (1979); G. Passarino and M. Veltman, *ibid.* **B160**, 151 (1979).

Figure Captions

Figure 1: Feynman diagrams contributing to selectron pair production in electron-positron annihilation. Pairs of the same type, $\tilde{e}_L^+ \tilde{e}_L^-$ or $\tilde{e}_R^+ \tilde{e}_R^-$, are produced through diagrams (a) and (b). On the other hand, pairs of a different type, $\tilde{e}_L^+ \tilde{e}_R^-$ or $\tilde{e}_R^+ \tilde{e}_L^-$, are produced through diagram (b) only.

Figure 2: Sneutrino mass as a function of the lightest selectron mass for $\mu < 0$ and (a) $\tan \beta = 2$, (b) $\tan \beta = 10$, and (c) $\tan \beta = 25$. In each case, different curves characterized by a constant value of the lightest neutralino mass are presented, as indicated in the figure. The experimental bound $m_{\tilde{\nu}} > 41.8$ GeV appears as a horizontal dotted line, and the bound $m_{\tilde{e}^\pm} > 45$ GeV is visible only in case (a) as a vertical dotted line.

Figure 3: Lightest stau mass as a function of the \tilde{e}_R^\pm mass for $\mu < 0$ and (a) $\tan \beta = 2$, (b) $\tan \beta = 10$, and (c) $\tan \beta = 25$. In each case, the curves are labeled by the same values of the lightest neutralino mass as in Fig. 2. In case (a), the stau mass turns out to be independent of the neutralino mass, therefore, the five curves appear superimposed. The horizontal dotted lines correspond to the experimental lower bound $m_{\tilde{\tau}^\pm} > 45$ GeV.

Figure 4: Mass of the lightest top (solid line) and bottom (dashed line) squarks as a function of the \tilde{e}_R^\pm mass for $\mu < 0$ and (a) $\tan \beta = 2$, (b) $\tan \beta = 10$, and (c) $\tan \beta = 25$. The curves are labeled by the value of the χ_1^0 mass as in Fig. 2.

Figure 5: Mass of the CP-odd (solid), charged (dashes), and heavy CP-even (dot-dashes) Higgs bosons as a function of the \tilde{e}_R^\pm mass for $\mu < 0$ and (a) $\tan \beta = 2$, (b) $\tan \beta = 10$, and (c) $\tan \beta = 25$. The curves are labeled by the value of the χ_1^0 mass as in Fig. 2.

Figure 6: Lightest CP-even Higgs mass as a function of the \tilde{e}_R^\pm mass for $\mu < 0$ and (a) $\tan \beta = 2$, (b) $\tan \beta = 10$, and (c) $\tan \beta = 25$. The curves are labeled by the value of the χ_1^0 mass as in Fig. 2.

Figure 7: Total cross section for the production of a pair of right selectrons in e^+e^- annihilation as a function of the \tilde{e}_R^\pm mass for $\mu < 0$ and (a) $\tan \beta = 2$, (b) $\tan \beta = 10$, and (c) $\tan \beta = 25$. In case (c) the dashed-dotted line indicates that the corresponding prediction for the $\text{BR}(b \rightarrow s, \gamma)$ is excluded. The curves are labeled by the value of the χ_1^0 mass as in Fig. 2.

Figure 8: Inclusive branching ratio of the decay $b \rightarrow s\gamma$ as a function of the \tilde{e}_R^\pm mass for $\mu < 0$ and (a) $\tan \beta = 2$, (b) $\tan \beta = 10$, and (c) $\tan \beta = 25$. The curves are labeled by the value of the χ_1^0 mass as in Fig. 2. CLEO upper and lower bounds are shown as horizontal dotted lines, and the SM prediction appears as an horizontal

dashed line. The dashed–dotted line in case (c) is excluded even after considering the 25% theoretical error.

Figure 9: Branching ratios of the decay of a right selectron into neutralinos and an electron as a function of $m_{\tilde{e}_R^\pm}$. We consider $\mu < 0$ and take different values of $\tan\beta$ and the universal gaugino mass $M_{1/2}$. Only (a) χ_1^0 and (b) χ_2^0 are light enough for the decay to be allowed.

Figure 10: As a function of the selectron mass, we plot (a) the total cross section of selectron pair production, and (b) the branching ratio of the inclusive decay $b \rightarrow s\gamma$, for the case $\mu > 0$. Each curve is labeled by the values of $\tan\beta$ and $m_{\chi_1^0}$. Some of the solid curves in (a) are not plotted in (b) because their corresponding prediction for the BR is far above the upper limit we have set on the y-axis, although still compatible with the experimental limit if we allow for the 25% error quoted for the theoretical calculation. On the contrary, the dashed–dotted lines are excluded even after considering this error.

Figure 11: Total cross section for the production of a pair of right selectrons in e^+e^- annihilation as a function of the lightest neutralino mass. The curves are defined by a constant value of the right selectron mass and a constant value of $\tan\beta$ as indicated by the figure. Solid lines correspond to $\mu < 0$ while dashed lines correspond to $\mu > 0$.

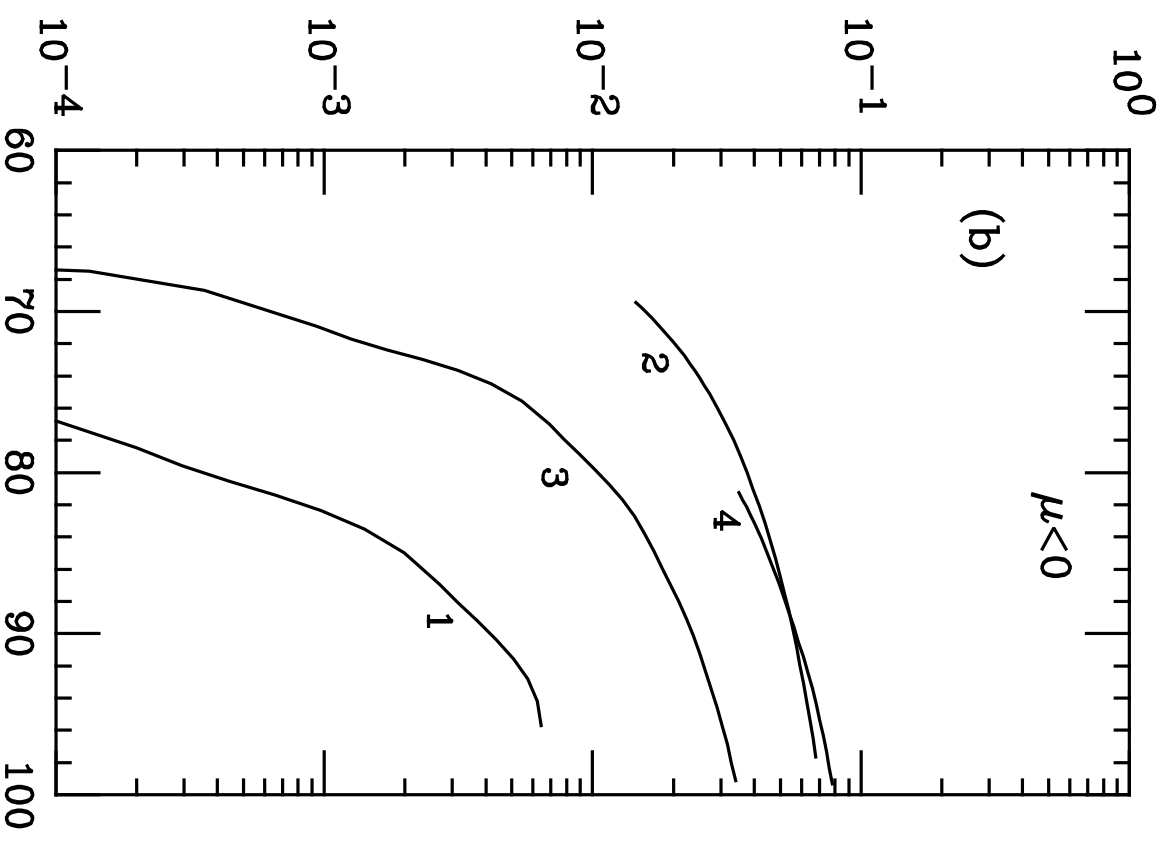
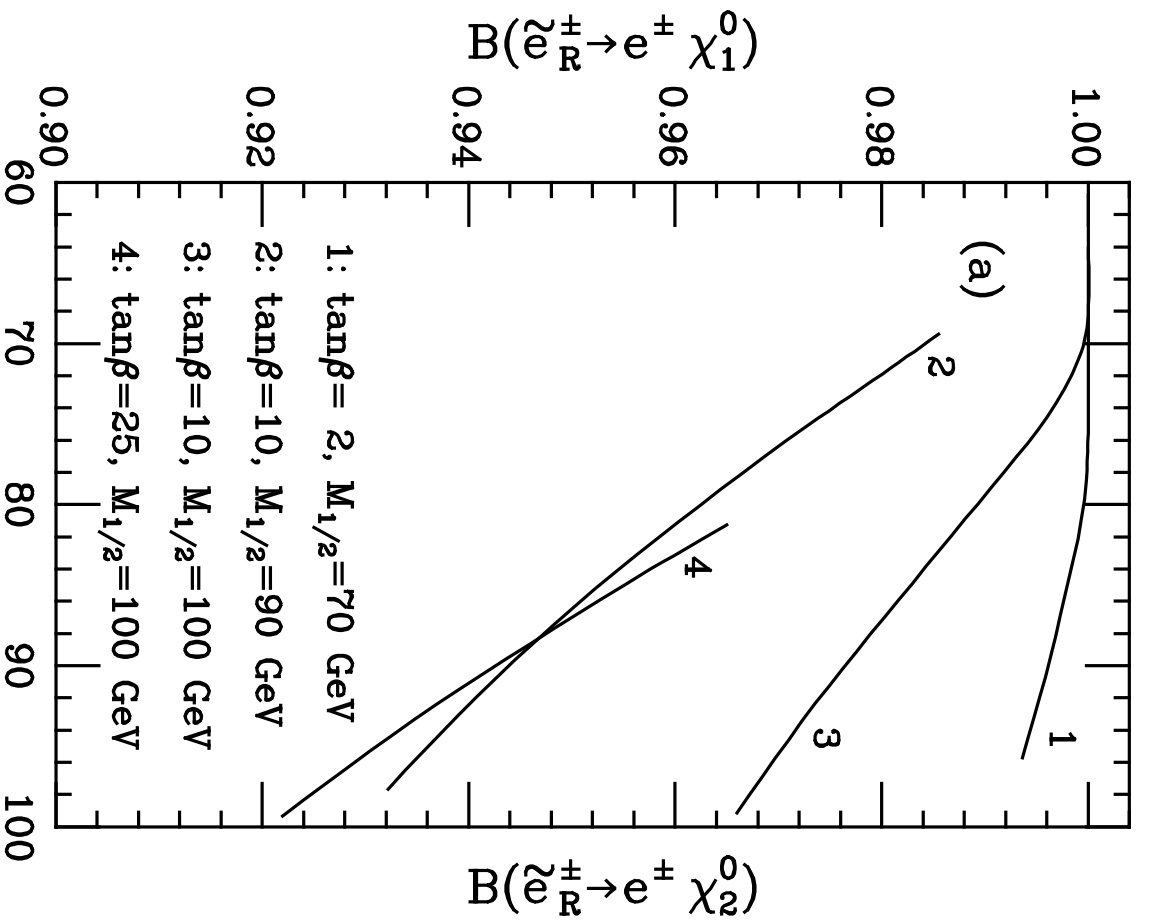


Fig. 9

$m_{\tilde{e}_R^\pm}$ (GeV)

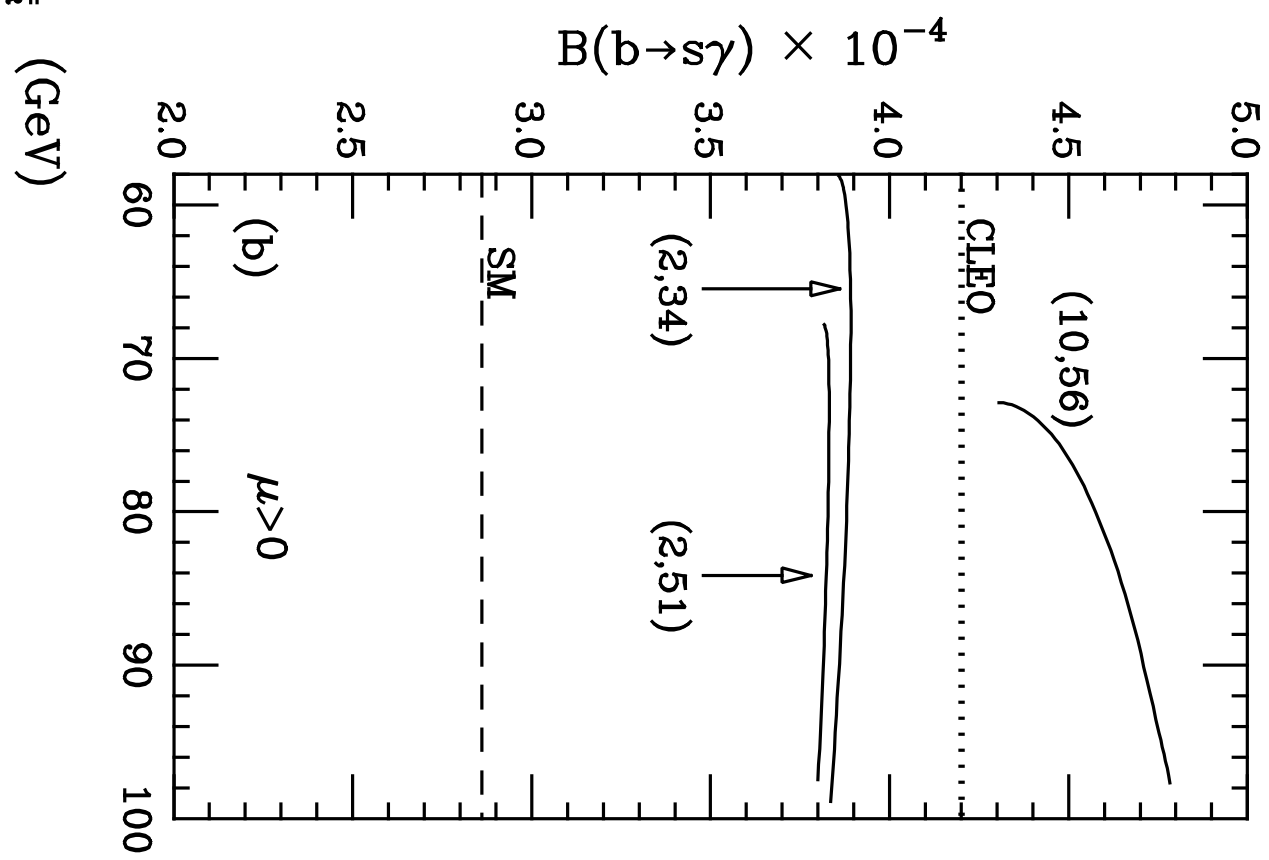
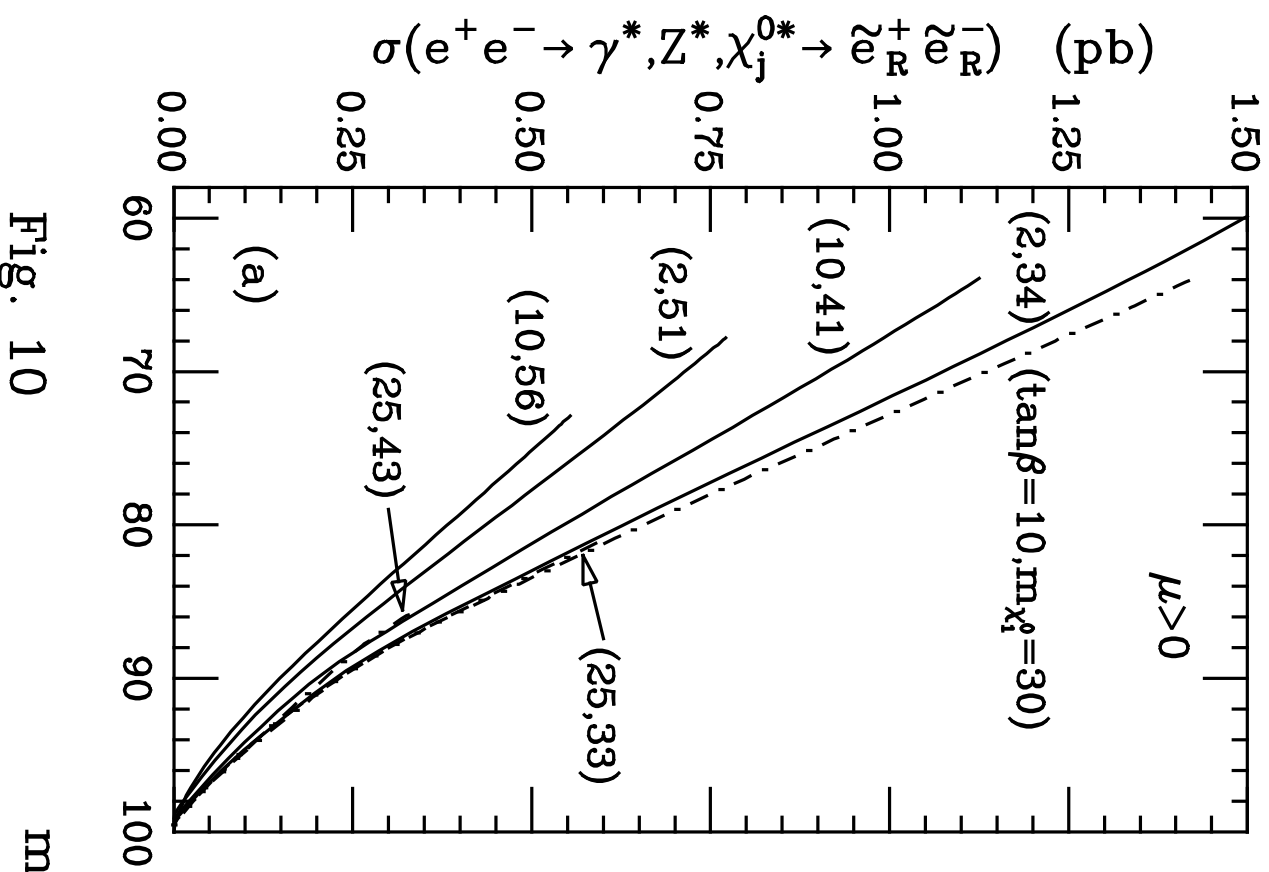


Fig. 10

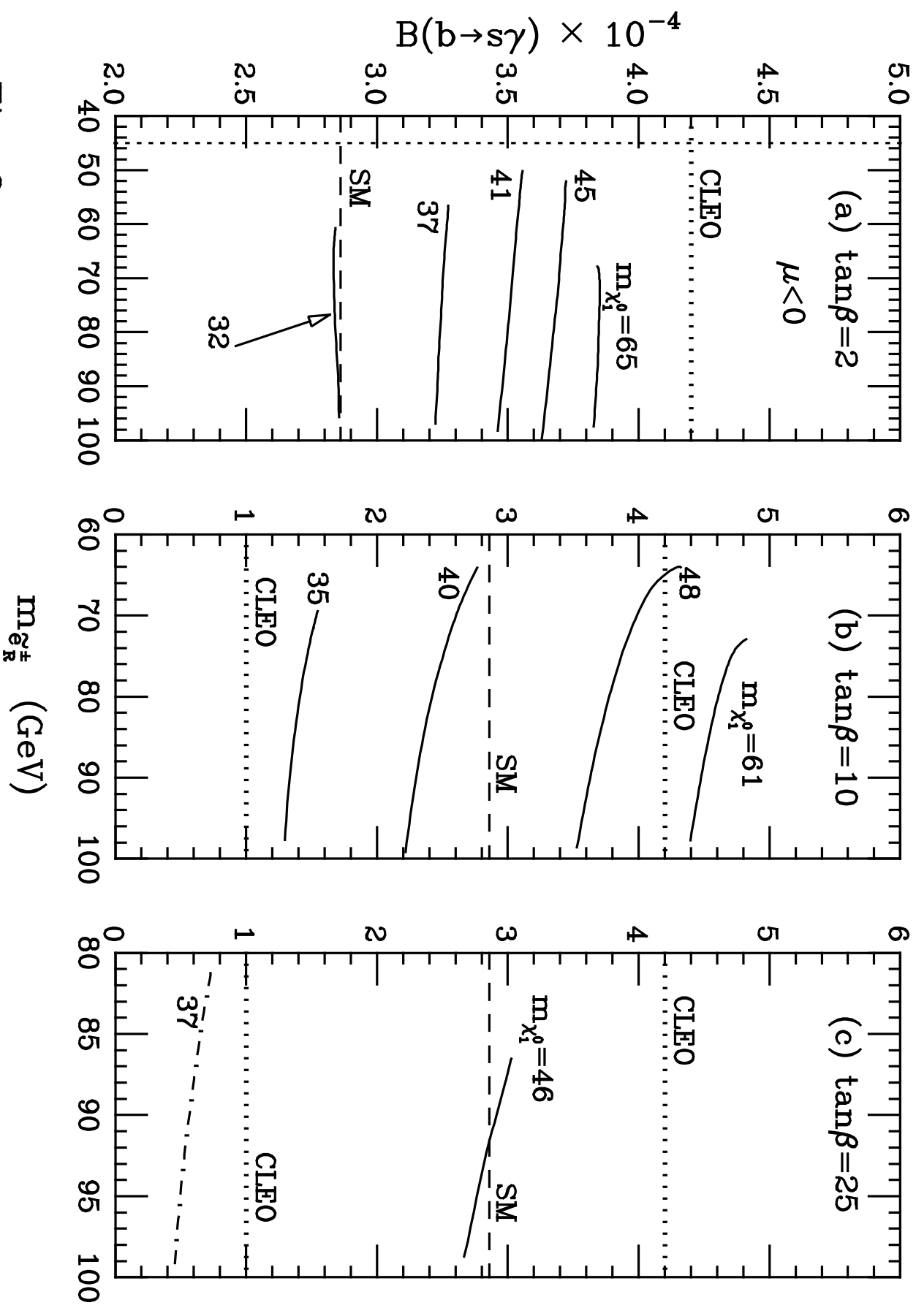


Fig. 8

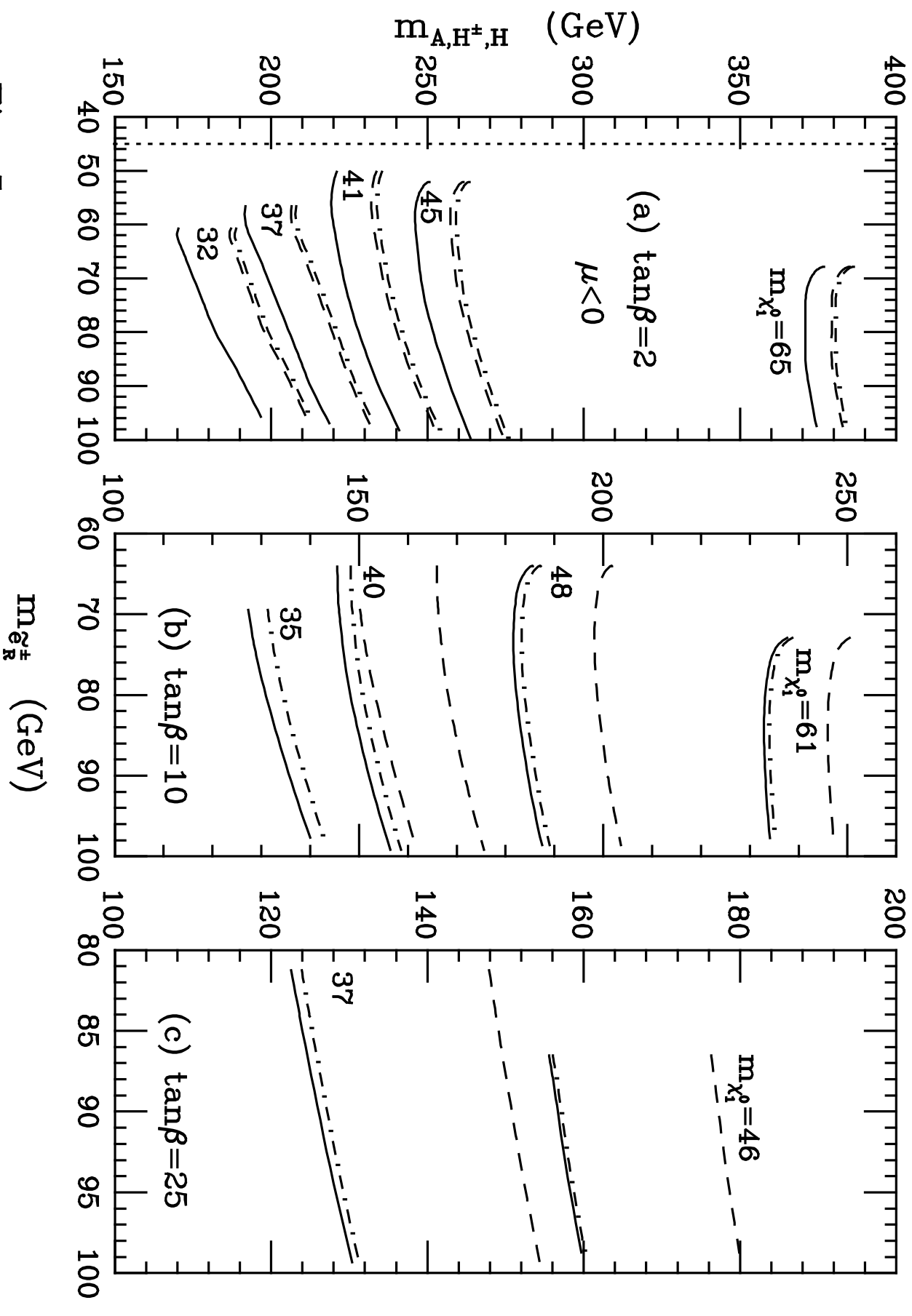


Fig. 5

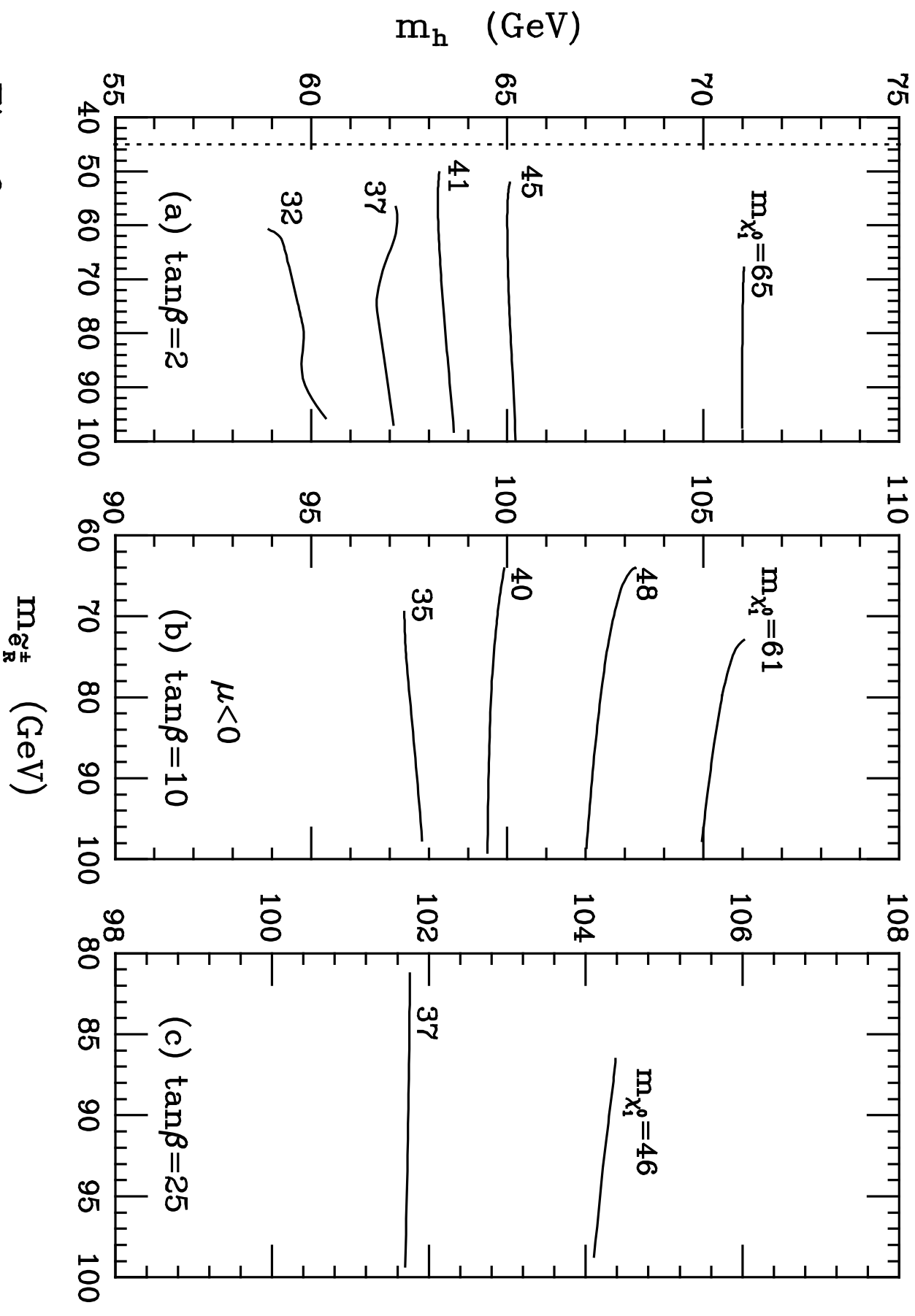


Fig. 6

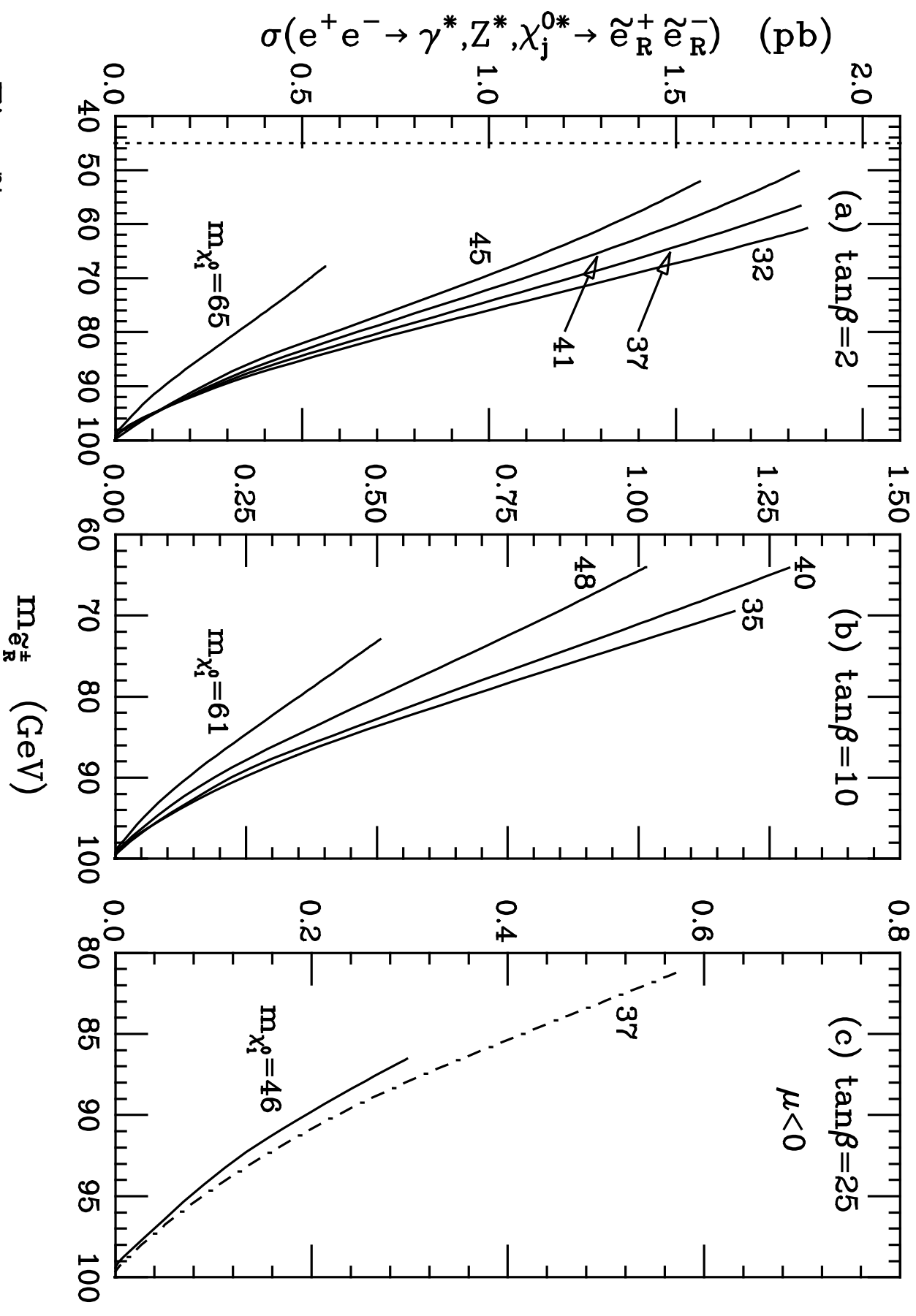


Fig. 7

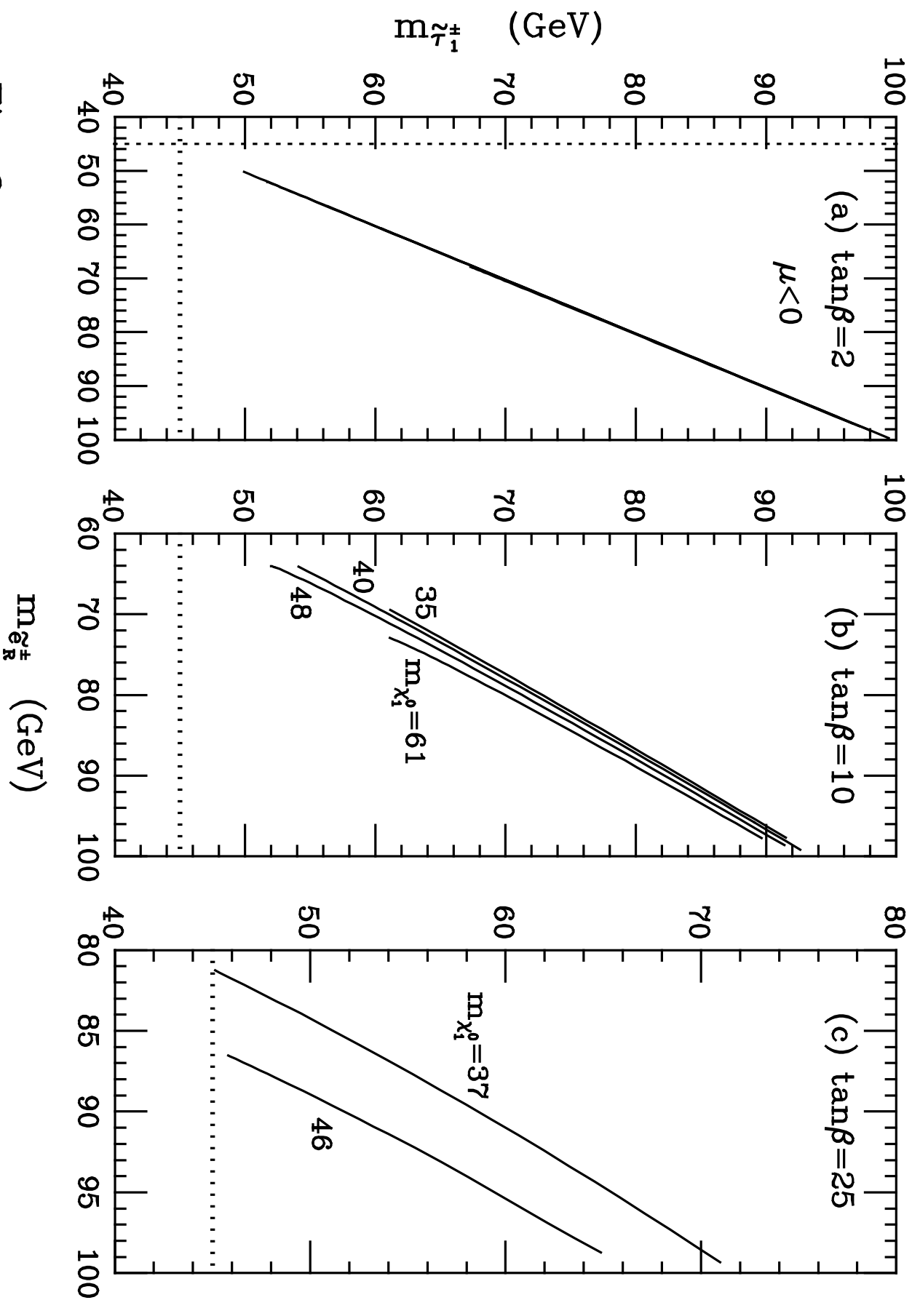


Fig. 3

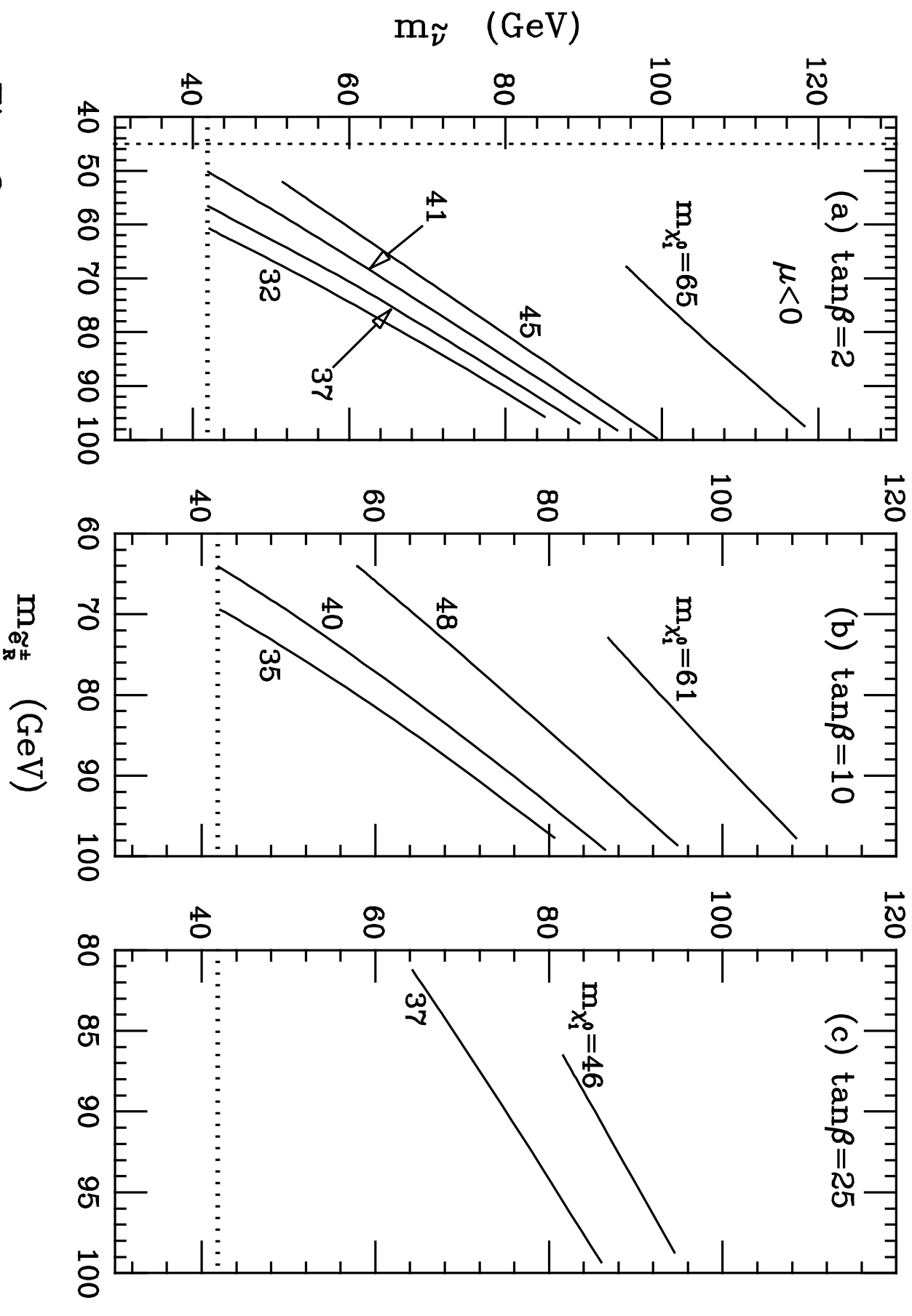


Fig. 2

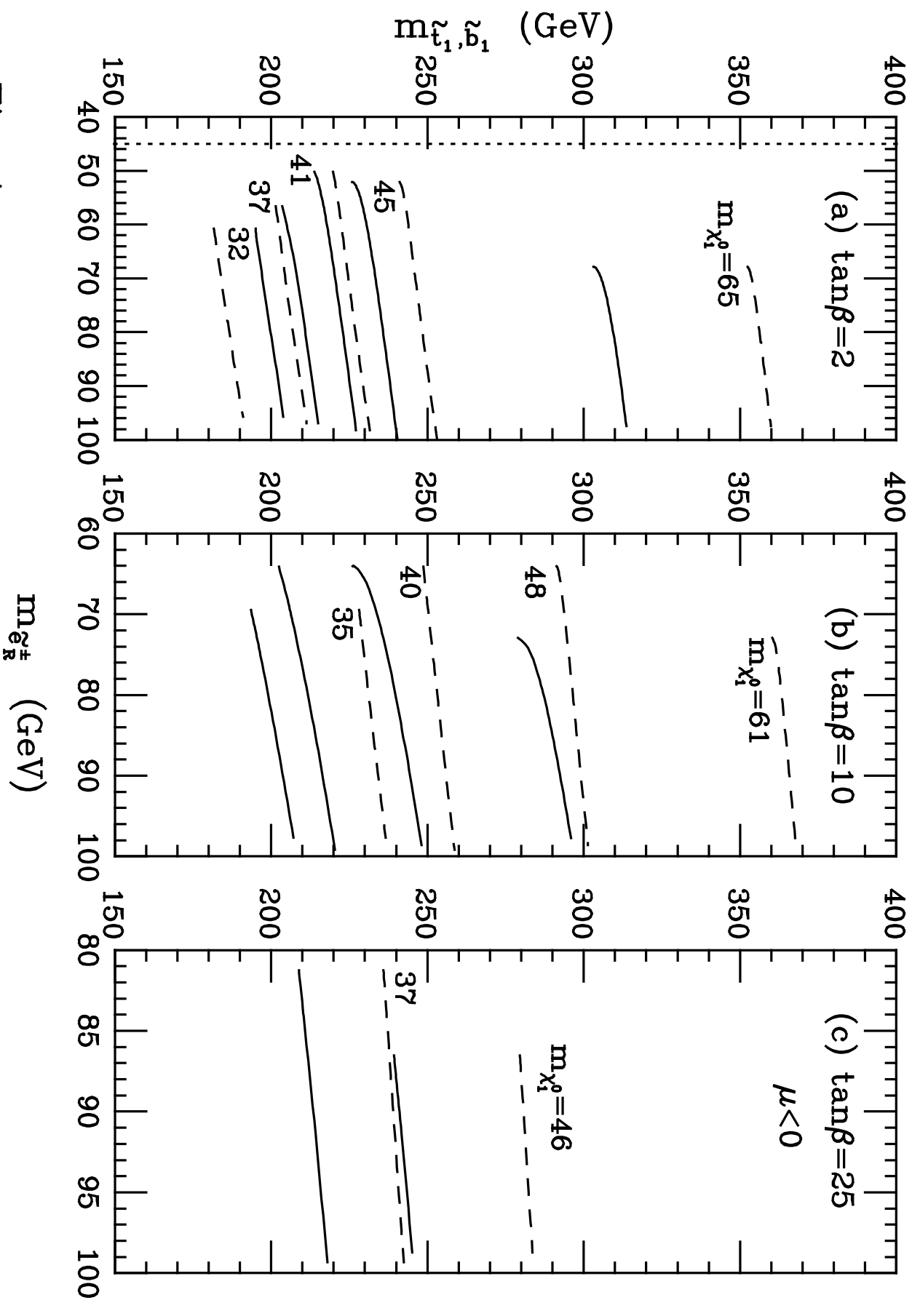


Fig. 4

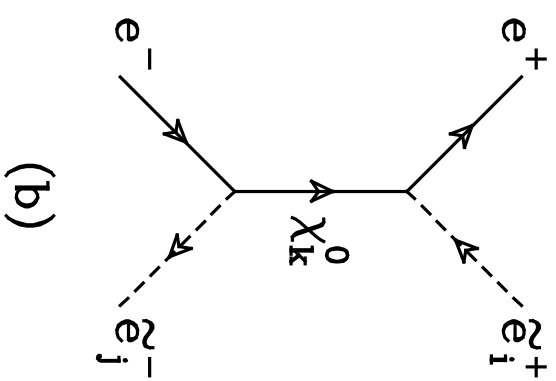
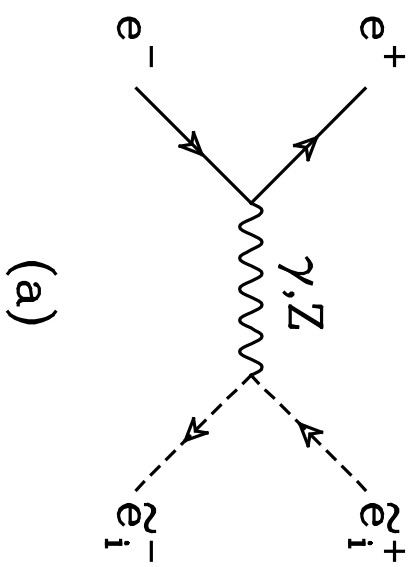


Fig. 1

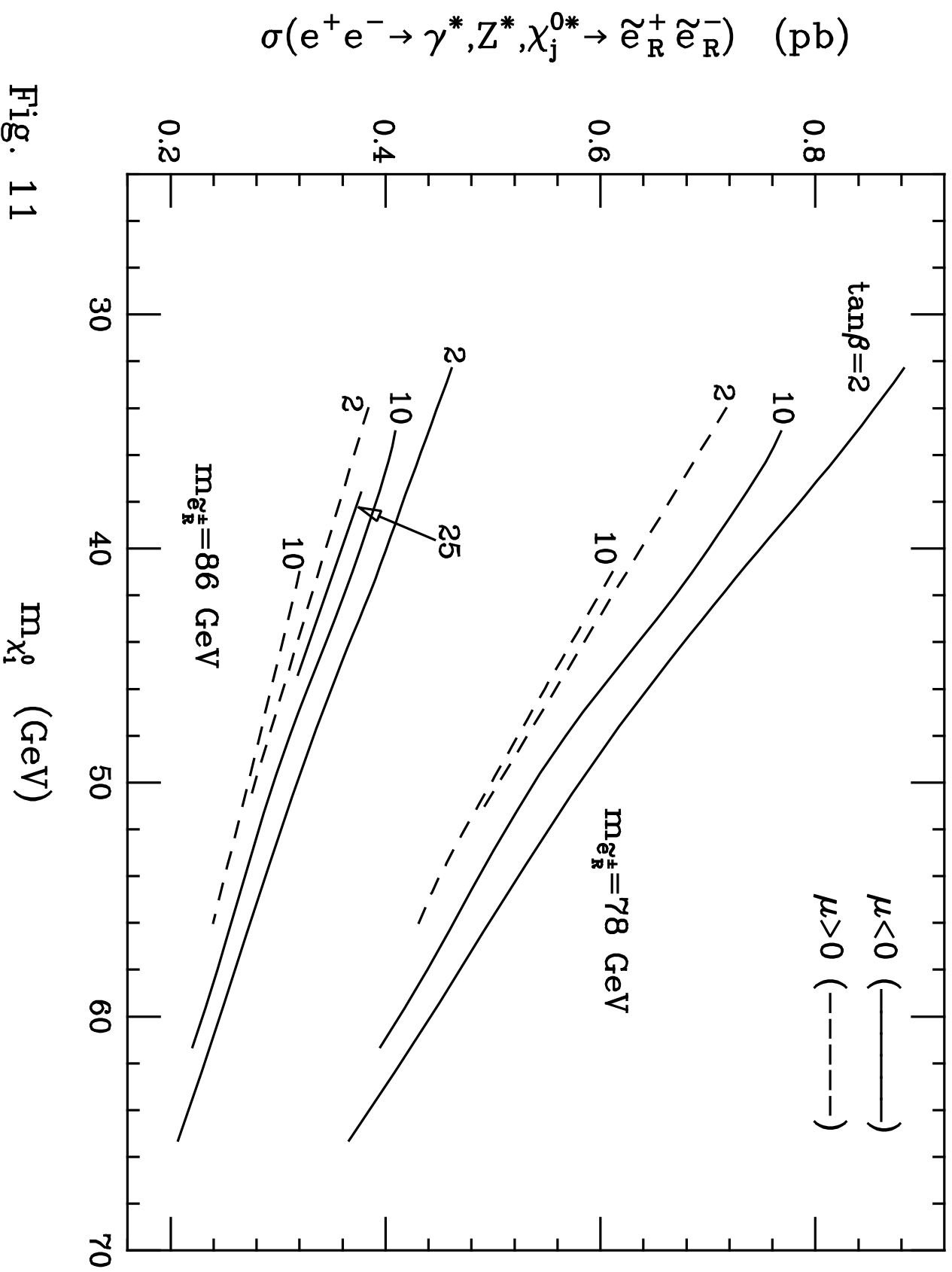


Fig. 11